Frontiers in Scientific Research and Technology

Online ISSN: 2682-2970
Print ISSN: 2682-2962
http://fsrt.journals.ekb.eg

FSRT J 11 (2025) 51 – 70 10.21608/fsrt.2025.376943.1159

The Role of Photothermal Nanocomposites in Next-Generation Membrane Distillation Technologies: A Review

Mohamed S. Fahmi[1,*], Ahmed Shahat[1], Mohamed E. A. Ali[2]

[1] Chemistry Department, Faculty of Science, Suez University, P.O. Box: 43221, Suez, Egypt

[2] Egypt Desalination Research Center of Excellence (EDRC), Hydrogeochemistry Department, Desert Research Center, Cairo, 11753, Egypt

ARTICLE INFO

Article history:
Submitted 19 April 2025
Received in revised form 29 April 2025
Accepted 1 May 2025
Available online 4 May 2025

Keywords
Photothermal membrane distillation,
polymeric membranes,
renewable energy,
Photothermal nanomaterials,
water desalination.

ABSTRACT

Communities worldwide face significant challenges pertaining to the scarcity of clean water sources and water pollution, necessitating the exploration of effective solutions such as desalination technologies. In recent years, conventional membrane distillation (MD) processes have undergone substantial advancements, particularly through the diversification of system designs and improvements in polymeric membrane properties. In this context, one interesting method is photothermal membrane distillation (PMD). That harnesses renewable light energy to enhance desalination efficiency. One of the most significant developments in this field is the integration of nanomaterials and carbon-based materials with photothermal properties into commonly used polymeric membranes including polyvinylidenefluoride (PVDF), polytetrafluoroethylene (PTFE), polypropylene (PP) and polysulfone (PSF). This integration aims to improve thermal performance, increase water production efficiency, and reduce energy consumption. These modifications have demonstrated remarkable success in boosting productivity and directly utilizing solar energy as a sustainable power source. With continued advancements, PMD technology is anticipated to perform a crucial role in providing clean water to areas without access to conventional sources of energy, making it a promising solution for future desalination strategies.

1. Introduction

Water pollution is increasingly acknowledged as one of the significant challenges of the 21st century. Various pollution sources, including domestic and industrial wastewaters, are escalating contamination levels [1]. Additionally, freshwater scarcity, made worse by population increase, climate change, and agricultural and industrial demands, has become a crucial societal issue. In response to these challenges, membrane technologies are being incorporated into water treatment processes. Popular membrane types used for seawater treatment include ultrafiltration (UF), microfiltration, reverse osmosis (RO) and nanofiltration (NF). These technologies can be used separately or in combination as hybrid systems. A promising solution to address these problems is (MD), a technique that offers substantial reductions in energy consumption, waste generation, and treatment costs while enhancing sustainability and safety [2]. MD, a hybrid thermal-membrane process, presents a potential advantage by overcoming the shortcomings of traditional desalination techniques through the synergistic exploitation of the water-energy nexus [3].

* Corresponding author at Suez University

E-mail addresses: m.shahat1286@gmail.com (Mohamed S. Fahmi)

Initially introduced by Bodell in the 1960s as a method for producing clean water using micro-porous hydrophobic membranes [2], MD did not gain significant attention until the early 1980s [3, 4]. Since then, MD has emerged as a modern technique for production drinkable water from seawater and brackish at a reasonable cost [5–7]. Additionally, it serves as a complement to conventional technology for desalination likes as multistage flash distillation process (MSF) and (RO) technology [8, 9]. MD operates by removing water vapor from heated watery mixtures at temperatures lower than 100°C [10, 11].

It facilitates the use of renewable energy sources, including solar power, to elevate the temperature of the feed solution, making The MD uses an energy efficient alternative [9]. However, MD still faces challenges, including membrane pore wetting [12], temperature polarization [13, 14], strong opposition to the movement of water vapor because trapped air in the pores [15], and conductive heat loss [16, 17]. In MD, a hot feed and a cold distillate are separated by a porous hydrophobic membrane and the vapor pressure difference across the membrane drives the vapor flux, which leads to the generation of pure water upon condensation [18]. Common materials for MD membranes include hydrophobic polymers such as (PVDF), (PTFE), (PP) [19], and (PSF)

[20]. Vapor flux generation in MD can be expressed using the equation:

$J = k(P_1 - P_2)$ ..... (1)

where J represents the vapor flux ($m \cdot s^{-1}$), k denotes the water vapor permeability of the membrane ($m \cdot s^{-1}$. Pa^{-1}), and P_1 and P_2 correspond to the water-air interface vapor pressures (Pa) on the membrane's permeate and feed sides, respectively. MD presents numerous advantages in comparison to alternative techniques for thermal and membrane desalination, encompassing a reduction in electrical power consumption. Diminished mechanical property specifications for the membranes, reduced fouling tendencies attributed to low-pressure functioning, the capability to process a diverse spectrum of feed water salinities, and the application of low-grade thermal energy [21-23]. However, current solar MD systems face limitations that reduce their energy efficiency. One key issue is the use of external solar thermal collectors to heat the feed water, leading to significant heat loss during the transfer to the MD module [24]. Furthermore, the temperature polarization phenomenon as illustrating in Fig.1a, b, which occurs due to thermal efficiency is severely constrained by heat transport across the membrane, both conductive and latent. As a result, the temperature at the feed side membrane surface (T_1) being much lower than the bulk feed water temperature (T_f), and the temperature at the distillate side (T_2) being much higher than the bulk distillate temperature (T_p).

This phenomenon reduces the difference in vapor pressure across the membrane, which in turn diminishes the membrane flux J (Eq. 1). In certain instances, the coefficient of temperature polarization (αTP) can be as low as 0.3, reducing the effective driving force by 70% [25].

$$\alpha TP = \frac{T1 - T2}{Tf - Tp} \quad \text{..... (2)}$$

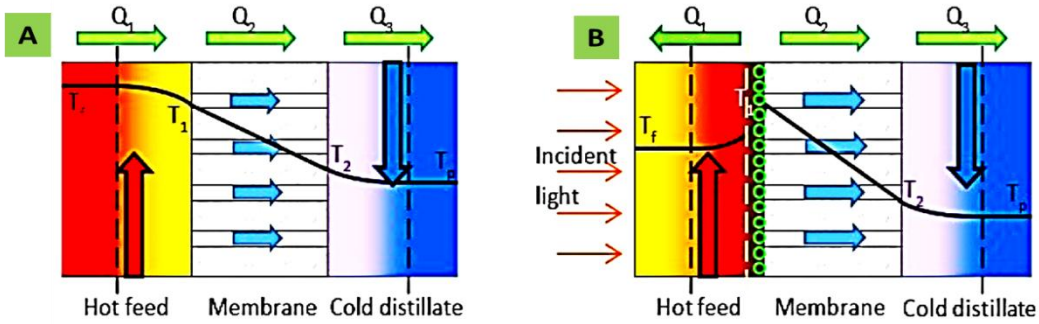

Figure 1. illustrates reduction of thermal polarization in conventional MD (a) system by photothermal MD membranes (b). Reproduced with permission from [26]. Copyright 2017 Materials Chemistry.

Photothermal membranes have demonstrated significant potential in enhancing MD processes. Ideal MD membranes are characterized by flexibility, lightweight construction, thinness, and hydrophobicity. Previous studies have integrated SiO_2/Au nanoshells and carbon black nanoparticles into commercial membranes to enhance their photothermal properties, showcasing exceptional photothermal properties [27].

A recent approach, nano-photonics-enabled solar membrane distillation (NESMD), employed a bilayer structure with a 25-μm photothermal nanocomposite electrospun layer (polyvinyl alcohol containing oxidized CB NPs) atop a PVDF membrane, achieving a flux of 0.22 $kg \cdot m^{-2} \cdot h^{-1}$ and solar efficiency >20% in small-scale modules [28].

PVDF membranes coated with silver nanoparticles under high-intensity UV irradiation also demonstrated an 11-fold flux increase in vacuum MD [29]. Additionally, scalable production techniques for photothermal MD membranes using CB NPs and SiO_2/Au NPs, yielding significant flux enhancements under 1 sun simulated sunlight [26].

These innovations provide promising pathways for clean water production in areas lacking reliable water and energy infrastructure.

2. Photothermal nanomaterials

Nanotechnology developments have made it possible to create photothermal materials, which convert low-density light energy into thermal energy. These materials are widely studied for applications in fields ranging from biomedicine to environmental science.

In biomedicine, near-infrared (NIR) light triggers the photothermal effect, which allows deep tissue penetration with minimal invasiveness. This has proven beneficial for cancer treatments, where NIR irradiation kills tumor cells while leaving healthy tissue intact [1, 4].

In a similar vein, NIR-responsive nanomaterials work well to combat bacterial infections by preventing bacterial development through heat and the production of biofilms. Additionally, photothermally active compounds are gaining attention for solar-driven vapor generation, such as in seawater desalination and wastewater purification, providing sustainable solutions for fresh water production. These materials harvest solar energy and convert it into thermal energy to heat water and generate steam [2, 3, 30, 31].

The NIR radiation (780–2500 nm) makes up nearly half of solar energy, and its utilization for water evaporation offers a green, low-energy solution.

Photothermal materials are divided into four primary categories, as shown in Fig. 2: plasmonic metals (such as Au and Ag), semiconductors (such as WO3, CuS), carbon-based nanomaterials (such as graphene and carbon nanotubes), and polymers (such as polyaniline and polypyrrole).

Various strategies have been developed to enhance their photothermal performance, resulting in progress across photothermal therapy, sterilization, and solar-powered water evaporation applications. [30, 32].

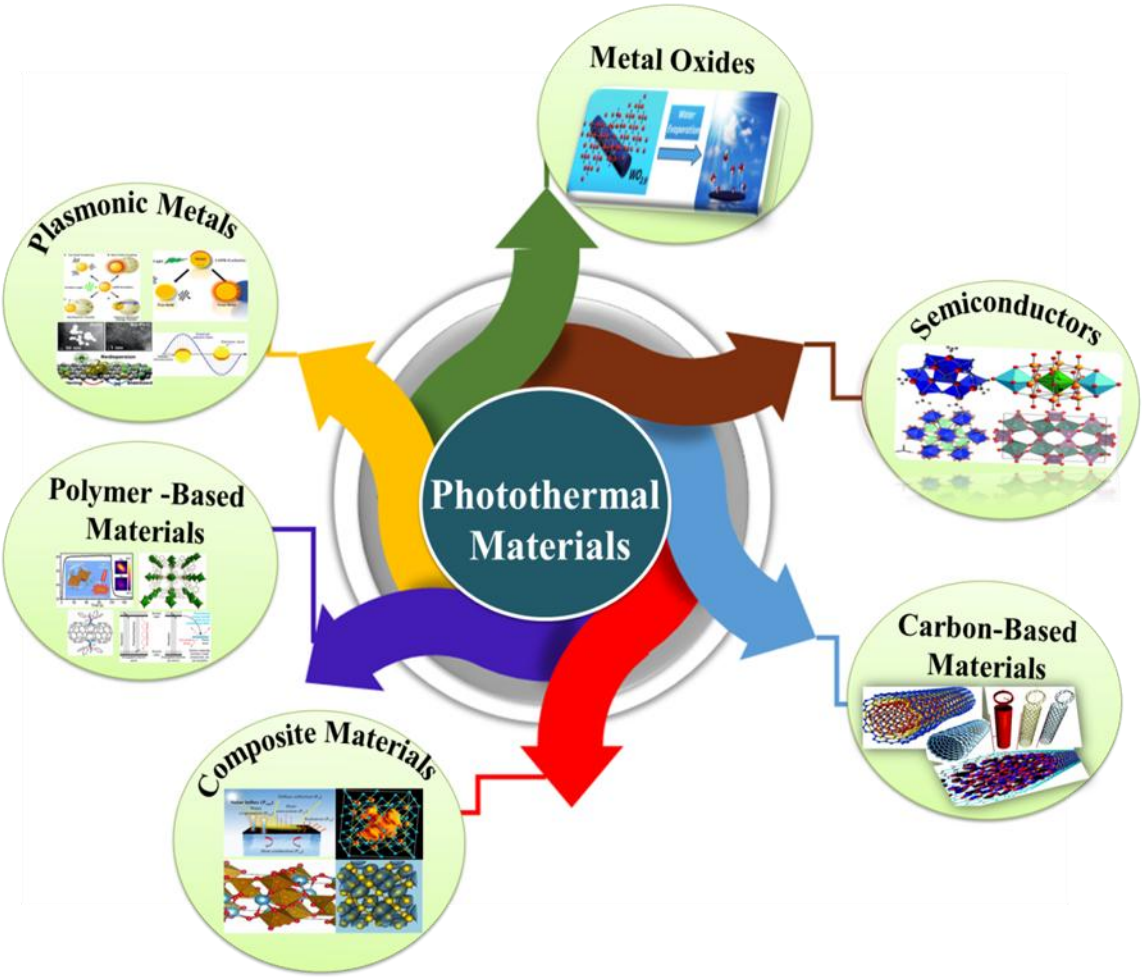

Figure 2. illustrates diagram for different types of photothermal nanomaterials.

2.1. Photothermal mechanisms

The photothermal effect is the process by which materials absorb light energy and convert it into heat, leading to a temperature increase [33]. Nanostructured photothermal materials enable localized heat modulation at the nanoscale, with conversion mechanisms divided into three primary categories, as shown in Fig. 3a: (1) plasmonic heating in metals; (2) electron–hole pair production and relaxation in semiconductors [34]. Metallic nanomaterials, such as gold and silver, have attracted significant interest due to their ability to interact with light in the NIR region. This interaction leads to the excitation of free electrons on the nanoparticle surface, resulting in localized surface plasmon resonance (LSPR) [35, 36]. LSPR decays through radiative and non-radiative pathways, with the latter generating hot electrons and inducing particle heating. Three main processes are involved in the decay kinetics of photoexcited gold nanoparticles: electron–electron scattering, (<100 fs), Phonon–phonon is scattering (about 100 ps) and electron–phonon scattering (1–10 ps) [37-39]. LSPR effects depend on elements like the size, content, shape, and surrounding dielectric medium of the particles [40]. While noble metals (Au, Ag) are commonly used, other plasmonic materials include transition metals (Al, Cu, Co, Ni), [41- 44], metal oxides (WO_{3-x}, MoO_{3-x}, [44- 47] and chalcogenides of transition metals (Cu_{2-x} E, E = S, Se) [48, 49]. (3) HOMO–LUMO excitation with lattice vibrations in molecules as illustrate in Fig. 3b. Organic photothermal materials have

gained attention for their efficient light-to-heat conversion and flexibility, yet challenges remain due to complex design and synthesis. As example to address this, an organic way to transfer charges co-crystal was created and added to polyurethane to improve its electrical conductivity and produce a large-area photothermal nanofiber membrane using electrospinning. It had high photothermal conversion efficiency (PCE) of 69.3% and a narrow energy gap of 0.33 eV. Transient absorption spectroscopy at femtoseconds showed that non-radiative transitions encompassing charge separation and internal conversion, contribute to its high efficiency. Under laser irradiation (0.183 W/cm²), the membrane rapidly reached 52 °C, demonstrating a PCE of 53.7%, so this study contributes to the development of large-area photothermal membrane fabrication and photothermal imaging applications as depicted in Fig. 3c [50].

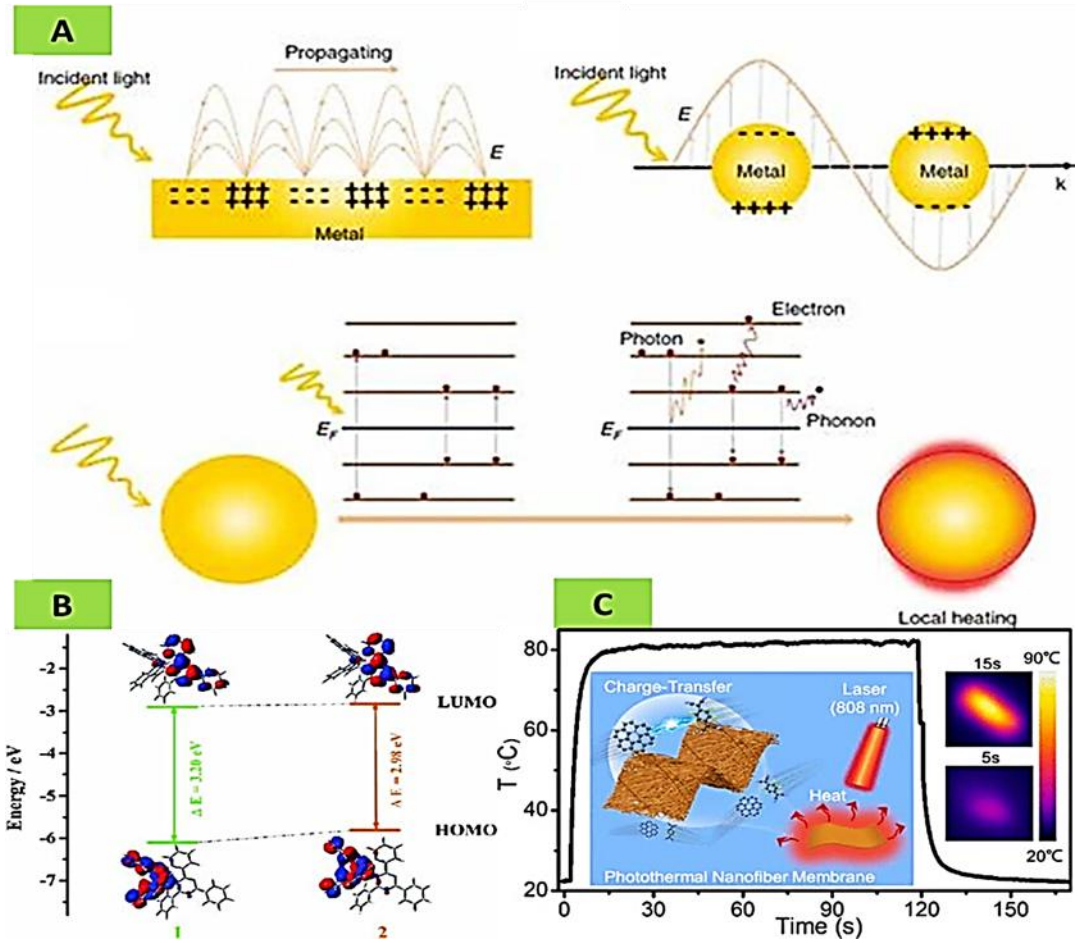

Figure 3. Diagrams illustrate (A) surface plasmon propagation, including surface plasmon generated (SPP) at the metal-dielectric interface, LSPR generated on metal nanoparticles, and surface plasmon decays that cause local heating in three different ways (photon-to-electron, electron-to-electron, and electron-to-phonon). Reproduced with permission from [34]. Copyright 2019 Nanophotonics, (B) HOMO–LUMO excitation and molecular lattice vibration (C) Under laser irradiation, the photothermal nanofiber membrane's temperature increases quickly. Reproduced with permission from [50]. Copyright 2022 ACS Nano.

2.2. Photothermal materials classification

2.2.1. Nanoparticles of plasmonic metal

Because of their LSPR, metals with plasmonic properties, including gold and silver show notable photothermal effects. The photothermal characteristics of triangular Ag nanoplates under NIR laser irradiation have been thoroughly investigated [51-54]. Au nanospheres, with an absorption band between 500–550 nm, show a red shift in LSPR as particle size increases [55]. Various Au nanomaterials, such as rods, shells, and hollow structures, can tune plasmon resonance to the NIR region for efficient thermal conversion [56- 59]. Gold nanorods, known for their anisotropic shape and high NIR absorption, are frequently used in photothermal applications, with the absorption maxima near 800 nm [60- 64].

The synthesis of branched Au nanostructures, like Au nanocrosses, has shown increased absorption efficiency compared to Au nanospheres or nanorods [65], especially in the longer wavelength range. Despite, the advantages of Au nanostructures, while renowned for their photothermal

properties, often face challenges related to photothermal stability and morphological integrity. Under high-intensity laser irradiation, these nanostructures can undergo shape transformations, such as tip rounding or transitioning from anisotropic to more thermodynamically stable spherical forms. Such morphological changes can diminish their optical properties and efficacy in applications like photothermal therapy and sensing [66- 68]. Palladium nanostructures have been created to get around this due to their higher melting point, offering better photothermal stability. Palladium nanosheets, for example, exhibit tunable LSPR absorption in the NIR region (826–1068 nm) and show a remarkable 52.0% photothermal conversion efficiency at 808 nm [69- 71]. Additionally, palladium nanocorolla, consisting of ultrathin nanosheets, demonstrates an enhanced photothermal effect, with a temperature elevation from 26.6°C to 50.4°C under 808 nm irradiant of Laser [72]. Palladium nanoparticles with a porous structure exhibit nearly double the NIR absorption of solid palladium nanocubes [73].

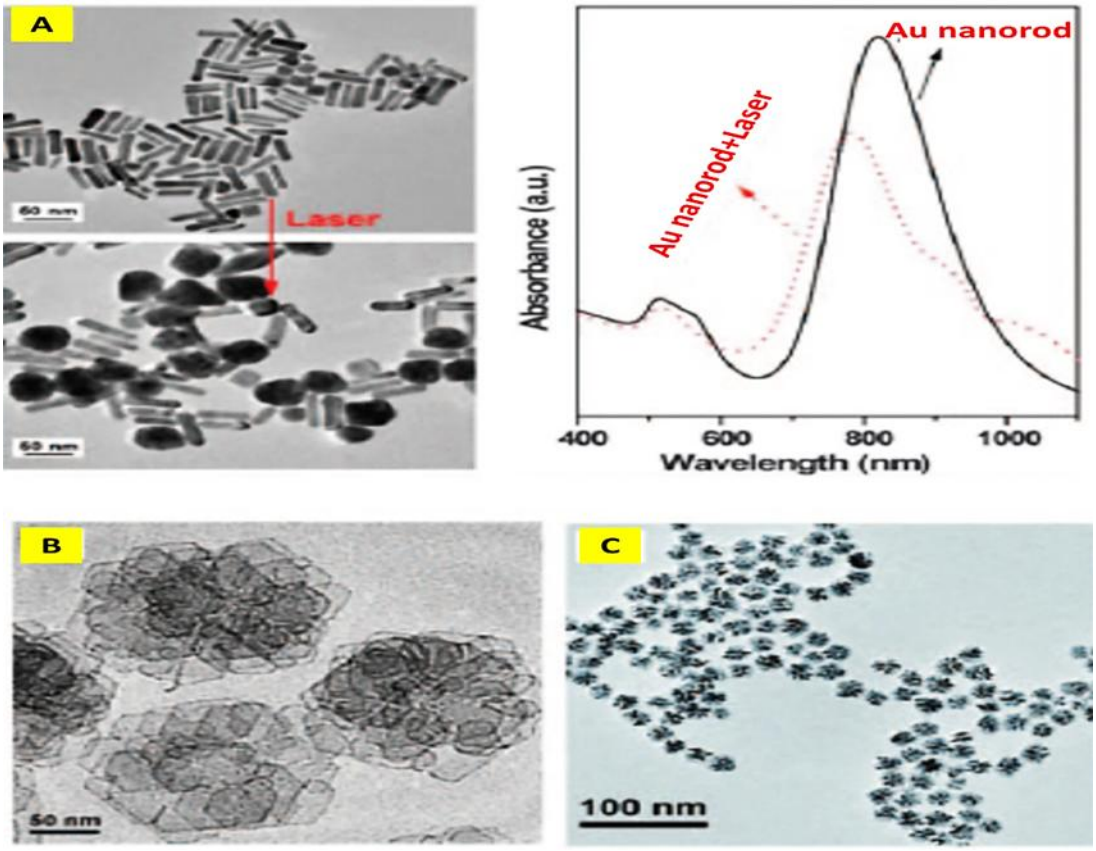

Figure 4. illustrates (a) Laser irradiation of Au nanorods for photothermal stability upon 980 nm (2 Wcm^{-2}, 30 min). Reproduced with permission from [67]. Copyright 2013 American Chemical Society, (b) TEM image of the palladium nanocorolla. Reproduced with permission from [82]. Copyright 2017 Chemistry of Materials, (c) TEM image showcasing porous palladium nanoparticles. Reproduced with permission from [73]. Copyright 2017 Nanoscale.

2.2.2. Semiconductors

Since they have high attenuation coefficients in NIR region, customizable absorption spectra, resilience to photo bleaching and degradation, ease of synthesis, and low cost, nanomaterials, especially metal oxides and chalcogenides have drawn a lot of interest [55]. Of them, copper sulfides ($Cu_{2-x}S$) have demonstrated exceptional promise for use in photothermal processes. From disks to spheres, different Cu_7S_4 nanocrystals perform exceptionally well in photothermal evaporation. Known for their broad-spectrum photo-absorption, hydrophobic $Cu_{12}Sb_4S_{13}$ nanoparticles exhibit excellent photothermal heating, which results in effective vapor formation [56]. For solar-driven evaporation, hierarchical copper phosphate (HCuPO) has also been documented [57]. Titanium-based semiconductors, such as narrow-bandgap Ti_2O_3 [79], black TiO_2 [60], and black TiO_x [59], have been utilized as innovative light absorbers to produce solar steam because they can absorb the whole spectrum of the sun. Magnetic particles that are inexpensive, non-toxic, and recyclable, such as Fe_3O_4, $MnFe_2O_4$, $ZnFe_2O_4$, and $CoFe_2O_4$, have also been employed enables extremely effective water evaporation over surfaces [63–65]. Moreover, other semiconductor materials, such as $BiInSe_3$ [24], SnSe [25], Al–Ti–O [61], NiO [62], and MoO_{3-x} [63], have been recognized and confirmed as efficient materials for catalysis or photothermal evaporation.

2.2.3. Materials based on carbon

Materials made of carbon offer several advantages over metallic materials and semiconductors, including lower cost, abundance, and outstanding ability to absorb light in a variety of wavelengths and convert light into heat with high efficiency [64, 75]. Various structures made of carbon, ranging from 1D to 3D configurations, have been created and developed for applications of photothermal (Fig. 5). For instance, 1D carbon nanotubes (CNTs) on silica (Fig. 5a and b) [76] and flexible wood substrates [65] have demonstrated high efficiency in solar-driven interfacial water evaporation. Graphene-based materials have been widely employed as light absorbers for processes including water evaporation, purification, and desalination because of its huge surface area, exceptional light absorption, and adjustable thermal conductivity [77- 79]. Various graphene-based compounds, such as porous graphene sheets doped with nitrogen (Fig. 5c and d) [80], graphene oxide (GO) films, Membranes made of graphene sheets oriented vertically (Fig. 5e, f) [4], Composite aerogels of reduced graphene oxide (rGO) and graphene (Fig. 5g) [68, 69], because of their specific structural characteristics, exfoliated graphite foam [71], hierarchical graphene foam [70], and both show outstanding water evaporation performance. Additionally, carbon-based compounds have been investigated for their photothermal qualities in water evaporation, including carbon black [3, 72, 73, 81, 82], hollow carbon beads (Fig. 5h) [83, 84], carbon fabric [85], carbon foam [86–88], carbon sponge (Fig. 5i) [31], and coke-derived carbon [89].

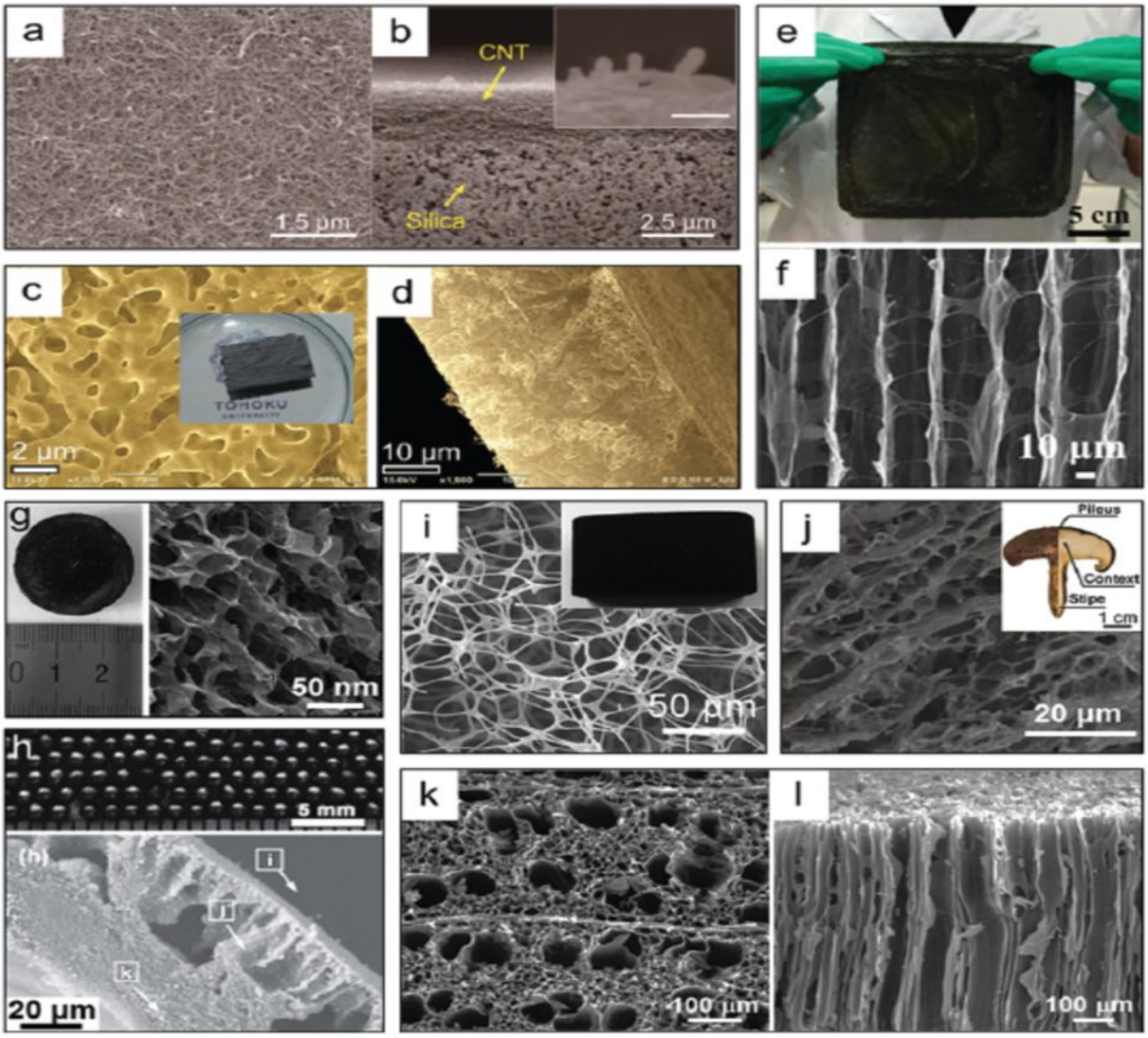

Figure 5. depicts digital SEM photos of a various materials based on carbon (a and b) carbon nanotubes on silica. Reproduced with permission from [76]. Copyright 2016 Nanoscale, (c and d) porous graphene sheet doped with nitrogen. Reproduced with permission from [80]. Copyright 2019 npj Computational Materials, (e and f) membrane made of graphene sheets oriented vertically (4), (g) Aerogel composite rGo. Reproduced with permission from [68]. Copyright 2019 Materials Today Energy, (h) Beads of hollow carbon. Reproduced with permission from [84]. Copyright 2017 Advanced materials, (i) carbon sponge. Reproduced with permission from [31]. Copyright 1967 Industrial & Engineering Chemistry Process Design and Development, (j) the carbonized mushrooms. Reproduced with permission from [90]. Copyright 2017 Proceedings of the National Academy of Sciences, and (k and l) wood. Reproduced with permission from [91]. Copyright 2018 Advanced Science.

2.2.4. Polymer-based materials

Organic polymeric materials, particularly conjugated polymers, have a high photothermal conversion efficiency, outstanding light-harvesting capacity, and superior biocompatibility. These macromolecules, which include donor–acceptor (D–A) structured polymers like polyaniline, polypyrrole, and polydopamine, have π-conjugated backbones and are a novel class of NIR-absorbing photothermal materials [92–96]. Crystalline porous polymers with extended structures are known as covalent organic frameworks (COFs). characterized by high thermal and mechanical stability, low density, and easy functional modification. COFs serve as ideal platforms for integrating functional nanoparticles [96- 98]. The COF–FeO_4 core–shell microspheres were created by Tan et al. with a highly organized shell structure, achieving 21.5% photothermal conversion efficiency and a high molar extinction coefficient [99]. The COF-CuSe nanocomposites that Hu et al. had produced 26.34% photothermal conversion efficiency when subjected to a laser with a wavelength of 808 nm [100].

Hybrid porous materials made comprising metal clusters or ions that have been cross-linked by organic ligands are known as MOFs, or metal-organic frameworks. Numerous MOF subfamilies, including HKUST-1, UiO-66, ZIF-8, CPO-27, Fe–MIL-101–NH_2, and IRMOF-3, have demonstrated the impact of photothermal energy [101]. Notably, d–d transitions in metal ion centers caused CPO-27–Ni to reach 167°C after 5 minutes of UV–vis irradiation. On the other hand, even after 30 minutes of irradiation, MOFs without absorption bands in this range showed only slight temperature rises. MOFs' photothermal characteristics have been used in solid-state modifications, solvent removal, and chemical activation [101, 102]. Furthermore, MOFs have been combined with polymers such as polyaniline for application in photothermal therapy [103].

3. MD principle

MD is a separating process that is driven by heat wherein only the feed/retentate's vapor molecules side make it through a hydrophobic porous membrane and are collected on the permeate/distillate side following condensation [104]. Stated differently, the vapor pressure differential between the membrane's two sides is caused by a temperature differential across the membrane surfaces. MD is characterized by a thermal driving force and a hydrophobic nature, which theoretically makes it possible to completely reject non-volatile substances as inorganic ions, colloidal entities, macromolecules, and other non-volatile compounds [105]. The performance of the MD system is primarily evaluated based on the quantity and quality of the permeate flow. However, the application of MD in industry remains limited due to challenges pertaining to low permeate flow rate, pore wetting, membrane, module design, flux decline, and unpredictable economic and energy costs [106]. The MD process mechanism is depicted in Fig. 1. permanent variations in pressure of vapor between the membrane's feed and permeate sides are necessary to preserve the water vapor pressure. Four distinct modes are depicted in Fig. 6(a-d): Distillation by Direct Contact Membrane (DCMD) [107, 108]; Vacuum Membrane Distillation (VMD) [109, 110]; Sweeping Gas Membrane Distillation (SGMD) [111, 112]; and Air Gap Membrane Distillation (AGMD) [113, 114]; AGMD and DCMD designs do not require an external condenser, unlike SGMD and VMD setups, because water vapor condensation occurs inside the membrane module. Seawater and brackish water desalination may be done with any MD setup [115, 116]. Nonetheless, desalination is most frequently accomplished by DCMD, AGMD, and VMD [117, 118].

3.1. Novelties and advancements in hybrid MD systems recently

MD has seen significant advancements through its integration with other technologies, leading to improved efficiency and product quality. Hybrid MD systems can be divided into two primary categories: (i) integration with other membrane processes and (ii) integration with various separation processes. In the first category, combining MD with UF has worked well in treating oily wastewater. Gryta et al. [134] implemented DCMD following UF, achieving a 99.9% removal of total dissolved solids. Similarly, Drioli et al. [135] combined MD with RO in order to desalinate, enhancing water recovery rates. The hybrid system achieved a recovery factor of about 87%, surpassing independent RO (40%) and MD (77%). In the second category, MD has been combined with processes like fermentation. Gryta et al. [136] studied a hybrid bioreactor/MD system for ethanol production, where MD removed fermentation byproducts, enhancing sugar conversion efficiency. Additionally, MD's compatibility with renewable energy sources has been explored. Khayet et al. [137] investigated coupling DCMD with nuclear reactors for desalination, confirming the feasibility of using nuclear-generated heat and electricity for water purification. Despite these laboratory and pilot-scale successes, further research is necessary to address obstacles impeding the MD's commercialization hybrid systems, a new direct solar MD method that, as shown in Fig. 7(a, b), use a covering of photothermal nanoparticles or doping to absorb sunlight and transform it into heat at the surface of the membrane, It acts as the MD process's thermal driving factor. This method greatly improves MD's energy efficiency while overcoming the main drawback of temperature polarization that arises in traditional MD methods [26,131].

A novel solar-driven MD (SDMD) process further enhances efficiency by utilizing photothermal nanoparticles to convert sunlight into heat at the membrane surface, reducing temperature polarization as illustrate in Fig. 1 [26]. In this context, Fe_3O_4/Polyvinylidene fluoride-co-hexafluoropropylene composite membranes (Fe_3O_4/PVDF-HFP) composite membranes exhibit strong interfacial adhesion and excellent solar absorption. This leads to increased transmembrane temperature and reduced vapor resistance, achieving about 99.99% salt rejection rate under 1 kW m^{-2} of sun radiation and a high permeate flow of 0.97 kg m^{-2} h^{-1}. With a 53% photothermal conversion rate, one of the highest reported the membrane also

demonstrated stable operation in a system at pilot scale, producing 21.99 kg m^{-2} h^{-1}, an 11% improvement over solar-free systems. These findings highlight the potential of SDMD for practical water purification applications [138].

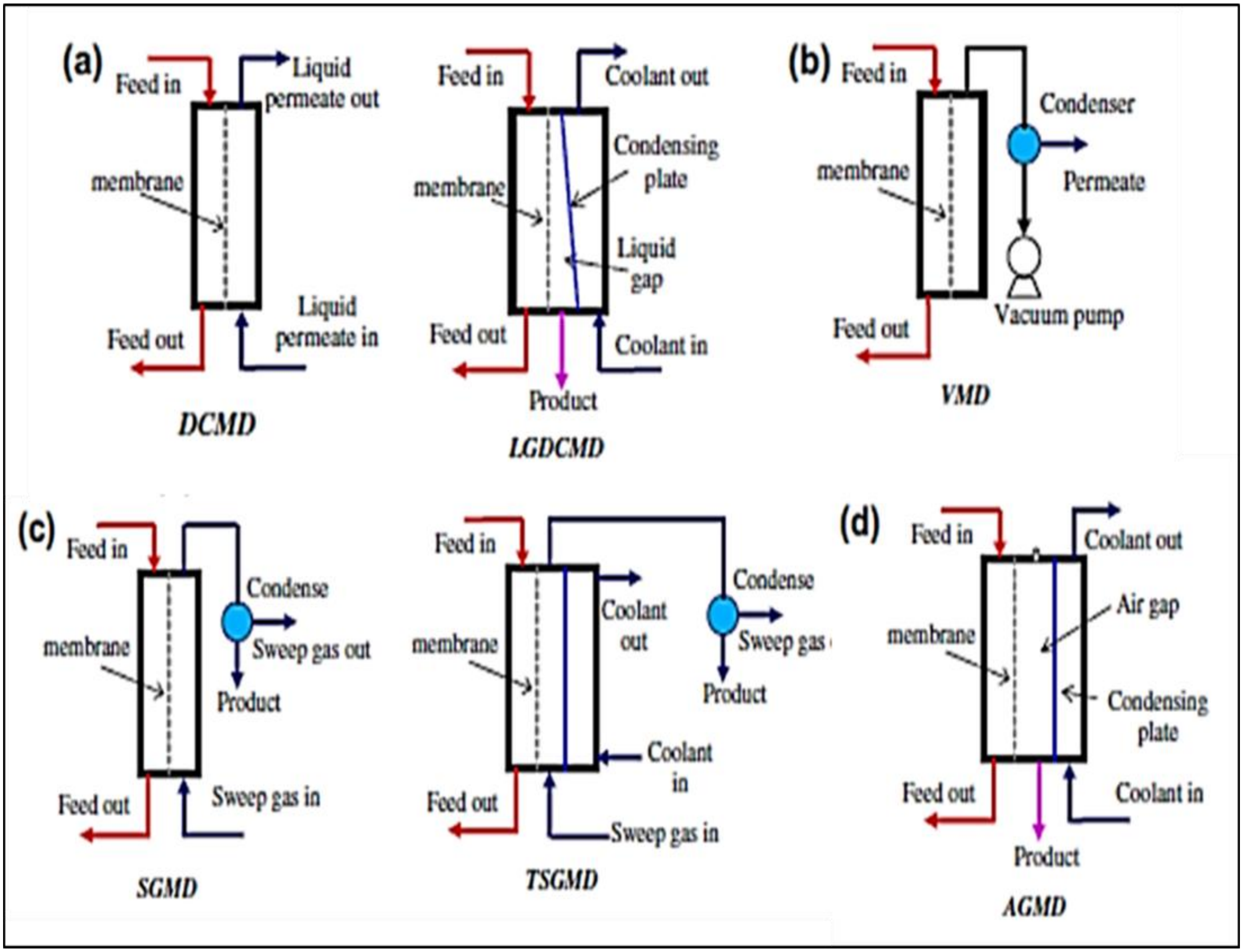

Figure 6. illustrates MD configurations: (a) DCMD and LGDCMD ; (b) VMD; (c) SGMD and thermostatic SGMD; (d) AGMD. Reproduced with permission from [119]. Copyright 2011 El-sevier.

3.2. Characteristics of MD membranes

To work at their best in the MD process, MD membranes need to have certain qualities. To avoid wetness during studies, the chosen membranes should be described using a variety of methods prior to doing MD testing. The main techniques for characterizing MD membranes are water contact angle, porosity, thermal conductivity, membrane thickness, and liquid entry pressure (LEP) [139].

3.2.1. Liquid entry pressure.

To prevent wetting of the membrane in the MD process, the membrane must simultaneously exhibit three key attributes: an elevated angle of contact with water, strong hydrophobicity, and a limited distribution of pore sizes. Wetting might still happen, though, if the solution of feed side makes direct interaction with the surface of membrane. If the transmembrane hydraulic pressure exceeds the LEP, the components of the aqueous solution overcome surface tension and penetrate the pores of membrane. LEP represents the highest pressure that can be applied to the input mixture prior to pore wetting.

The LEP value is established by the geometric coefficient (β), maximum pore radius (r_{max}), contact angle of surface (θ), and surface tension (γL), as per the Cantor-Laplace equation [140].

$$LEP = \frac{2\beta\gamma L\cos\theta}{r_{max}} \quad (3)$$

as inferred from the Cantor-Laplace equation, a rise in the angle of surface contact or reduction in the largest pore size will improve the LEP value.

Table 1: An overview of previous works on different MD configurations.

Membrane	Technique	Membrane properties	Configuration	MD conditions	Salt rejection (%)	Flux (kg/m^2 h)	Ref.
PSF/MWCNTs	Phase inversion	Θ: 82.3°	VEDCMD	NaCl: 2000–50000 ppm; T_f: 60 _C; T_p: 20 _C; Q_f : 5–35 L/min; Q_P: 1–7 L/ min; MA: 0.0019 m2.	99.99	41.58	[20]
PTFE	NA	Ɛ: 70%; δ: 175 mm; D_{avg}: 0.22 µm.	VEDCMD	NaCl: 0.6 g/L; v: 1.4 m/s; T_f: 40 _C; Tp: 20 _C; Ppv: 0.94 bar; MA: 12 cm2.	99.9	25	[120]
PTFE	NA	Ɛ: 75%; δ: 55–65 mm.	VEDCMD	NaCl: 35 g/L; Qf and QP: 1.0 L/min; Tf: 40 _C; Tp: 20 _C; MA: 118 cm2; feed/distillate pressure: 0.2/–0.6 bar.	NA	20.8	[121]
PTFE	NA	Θ: 127.5°; Ɛ: 70– 80%; δ:: 179 µm; D_{avg}: 0.2 µm.	VEDCMD	NaCl: NA; v: 1.1 m/s; T_f: 70°C; T_p: 24 °C; MA: 0.0168 m^2; P_{pv}: 0.3 bar.	NA	27.59	[122]
PTFE	NA	Θ: 160o; δ:: 10 µm; D_{avg}: 0.24 µm.	MGMD	Q_f and Q_P: 1.5 L/min; T_f: 80 °C; T_p: 20°C; water gap: 13 mm.	99.99	20.45	[123]
PTFE	NA	D_{avg}: 0.2 µm	V-MEMD	Q_f : 8–27.7 L/min; Q_P: 7.5 L/min; T_f: 60 °C; T_p: 25 °C; MA: 0.31 m^2.	NA	7	[124]
PTFE	NA	D_{avg}: 0.2 µm.	V-MEMD	Q_f: 69 L/h; T_f: 72 °C; P_{pv} : <0.2 bar; Total distillate collected: 99.6 L.	NA	NA	[125]
PTFE	NA	Ɛ: 70–75%; δ: 179 µm.	V-MEMD	NaCl: 1.0 M; Q_f : 40 L/h; T_f: 60 °C; MA: 0.16 m^2; P_{pv}: 0.1 bar.	99	9.4	[126]
PTFE	NA	Ɛ:%; δ: 40 µm; D_{avg}: 0.2 µm.	V-MEMD	NaCl: 60 g/L; Q_f : 50–70 L/h; T_f: 80°C; T_p: 26°C; Ppv: 40–80 mbar.	NA	NA	[127]
PP	NA	LEP: 1.4 bar; Ɛ: 70%; δ: 400 µm; Davg: 0.2 µm	MVMD	v: 2.4 m/s; Tf: 70°C; MA: 0.15 m^2; P_{pv}: 0.04 bar; Productivity: 3.97 m3/ day.	NA	NA	[128]
PP	NA	Ɛ: 68%; Davg: 0.2 µm.	MEMD	Q_f: 30 L/h; T_f: 85 °C; T_p: 35 °C; MA: 0.6 m^2.	NA	5.3	[129]
PTFE	NA	D_{avg}: 0.2 µm.	SPMD	Q_f: 69 L/h; Tf: 48.8 °C; MA: 0.32 m^2; P_{pv}: 113 mbar; Productivity: 70 L/ day.	NA	1.5–2.6	[130]
PSF/MWCNTs	NA	Θ: 112°	PDCMD	Q_f; 1.4 L/m, T_f=50 °C T_P=20±3 °C, NaCl= 2.0 g/L ,	NA	6.1	[131]
PTFE	NA	Ɛ: 70–75%; δ: 20 µm; D_{avg}: 0.2 µm.	V-MEMD	NaCl: 1.0 M; Q_f: 40 L/h; T_f: 60 °C; T_p: 25 °C; MA: 0.16 m^2; P_{pv}: 70 mbar.	99.9	13.42	[132]
TFE-co-VDF	NA	Ɛ: 70%; δ: 120 µm; D_{avg}: 0.25 µm.	LGMD	Q_f and Q_P: 250 L/h; T_f: 60 °C; T_p: 10 °C; MA: 0.0625 m^2.	NA	5	[133]

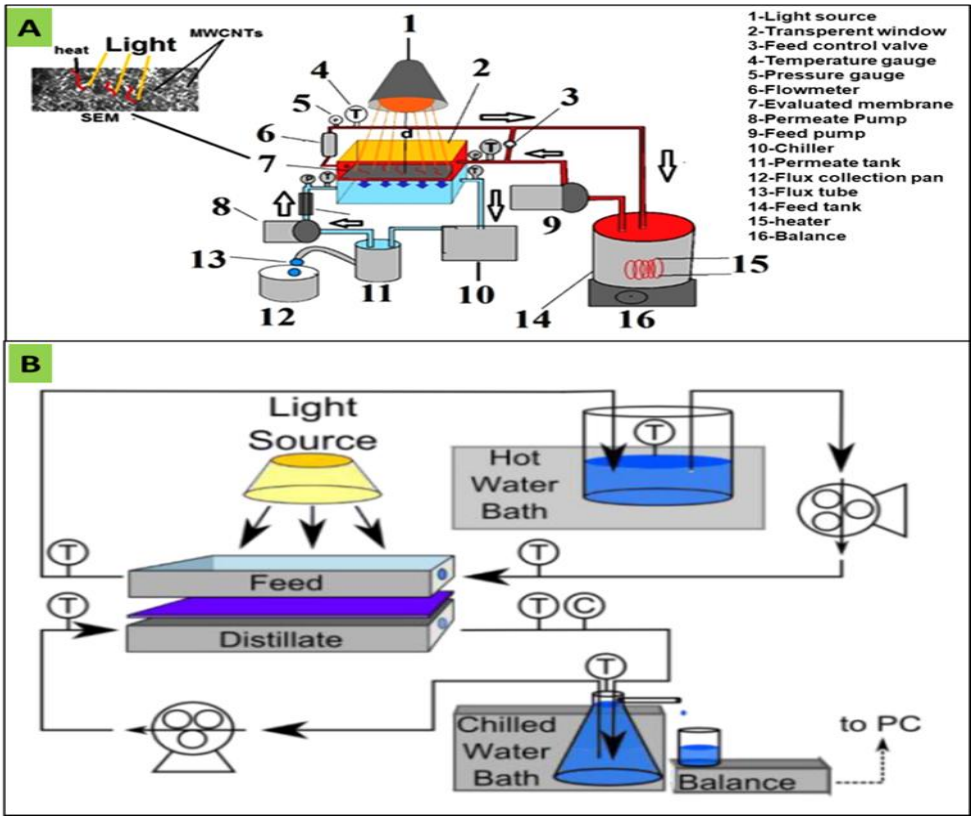

Figure 7. depicts (a) PMD system contain on PSF/MWCNTs photothermal membrane with transparent acrylic window. Reproduced with permission from [131]. Copyright 2024 Iranian Polymer Journal, (b) closed-loop solar MD system at the bench scale. The membrane module has a PVDF coated membrane with BC and a quartz window that allows light to pass through. Reproduced with permission from [26]. Copyright 2017 Materials Chemistry.

3.2.2. The porosity

The MD membranes' porosity need to be as high as feasible. without causing wetting. A porous surface increases the flow of permeate. In general, the ratio of free volume to the membrane's total volume is known as porosity. MD determines the porosity by computing the ratio between the macrovoids volume as well as the membrane's overall volume using a gravimetric method [141]. This technique includes determining the weight of the membrane before and after being completely soaked in a liquid that completely enters the pores, such 2-propanol.

$$\varepsilon\ (\%) = \frac{W_w - W_d}{\rho_{water} * A * L} \text{ x100} \quad \text{..... (4)}$$

where the membrane's wet and dry weights are denoted by W_w and W_d, respectively, ρ_{water} is the water's density, L is the membrane's thickness, while A is its surface area.

3.2.3. Water contact angle

The propensity of liquids to moisten a membrane surface is commonly assessed using analysis of liquid contact angles. In MD, as water is the primary a part of the feed cycle, the contact angle of water is measured to ascertain the surface's affinity for drops of water. This method involves calculating the angle created by a droplet of water and the membrane surface. To lessen calculation errors, multiple places on the membrane's surface that are randomly selected, as well as the average angle of contact is reported.

It is important to consider the effects of average pore size and surface roughness to accurately determine the contact angle of water as depicted in Fig 9(a-f).[139].

3.2.4. Conductivity of heat

The MD membranes should have the lowest possible heat conductivity. The primary causes of heat loss in various MD designs are the gases contained in the membrane pores and the membrane material. For the MD process, a decrease in mass flow may result from an increase in thermal conductivity.

Increasing membrane surface porosity can aid in reducing heat loss since water vapor has a much lower thermal conductivity than the polymeric materials used in MD. Therefore, reducing heat conductivity is facilitated by the membrane structure's macrovoids. As previously stated, the polymer's (kp) and the gases' (kg) thermal conductivity both affect the thermal conductivity of MD membranes.

$$k = \varepsilon kg + (1 - \varepsilon)K_p \text{..... (5)}$$

It's crucial to remember that the majority of the polymers used in MD membranes have comparable levels of heat conductivity. For instance, the thermal conductivity of polypropylene (PP) ranges from 0.11 to 0.16 W/m²·K, polytetrafluoroethylene (PTFE) from 0.25 to 0.27 W/m²·K, and polyvinylidene fluoride (PVDF) from 0.17 to 0.19 W/m².K [142].

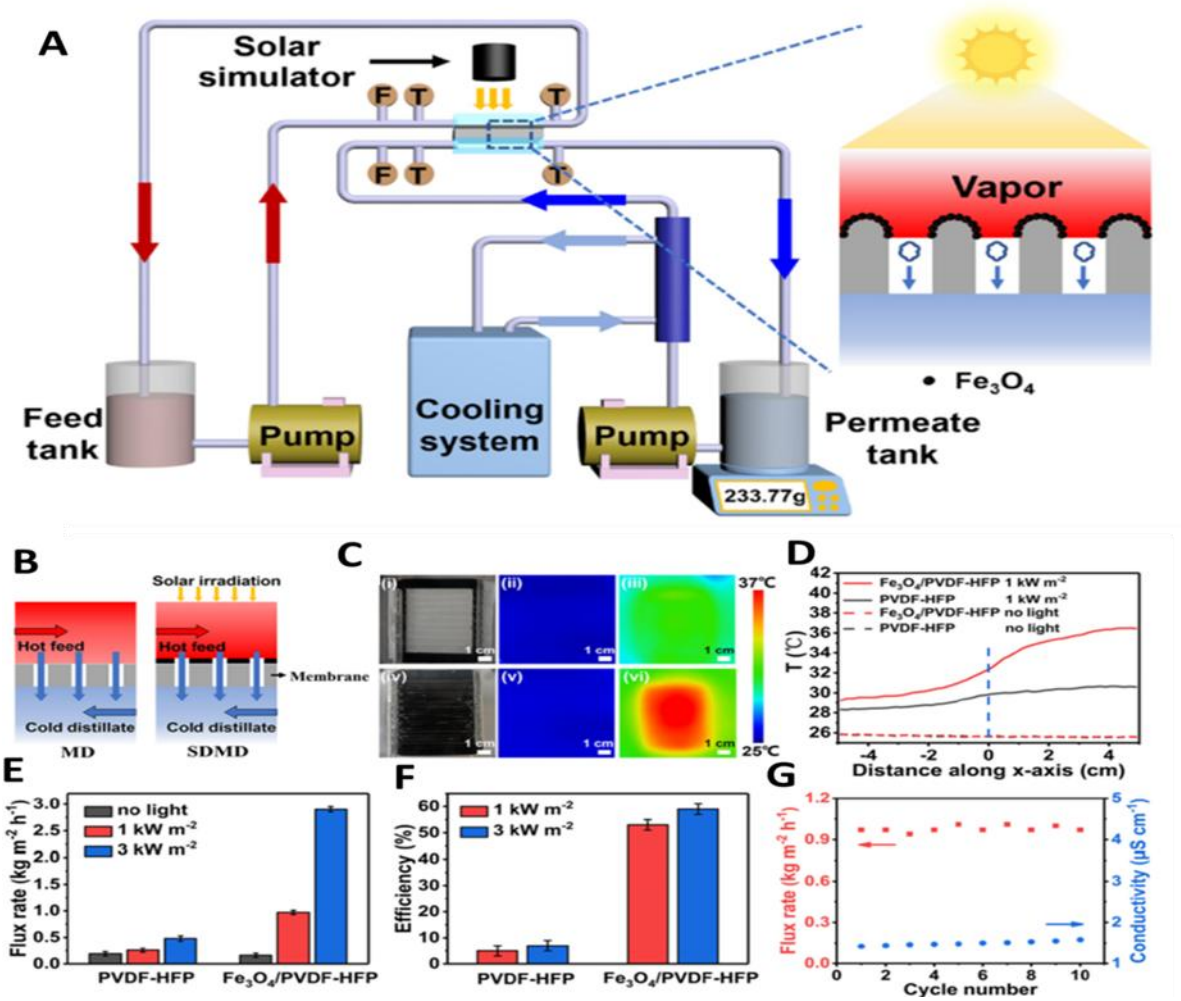

Figure 8. **(A)** The experimental setup schematic layout for SDMD **(B)** Diagram of conventional MD and new SDMD **(C)** Pictures of feed surfaces of membrane from PVDF-HFP (i) and feed surfaces of membrane from Fe_3O_4/PVDF-HFP; (iv) infrared camera pictures of PVDF-HFP membrane (ii) and Fe_3O_4/PVDF-HFP membrane (v) without solar light, PVDF-HFP membrane (iii), and Fe^3O^4/PVDF-HFP membrane (vi) under 1 kW m^{-2} irradiation density after 30 minutes of illumination; **(D)** Distribution of temperature of the membrane surface in the direction of the water flow; **(E)** Permeate flux of various membranes under varying solar irradiation; **(F)** Energy efficiency of various membranes under varying solar irradiation; an error bar represents the standard deviation. **(G)** Fe_3O_4/PVDF-HFP membrane permeability and conductivity performance throughout ten SDMD test cycles. Reproduced with permission from [138]. Copyright 2020 Desalination.

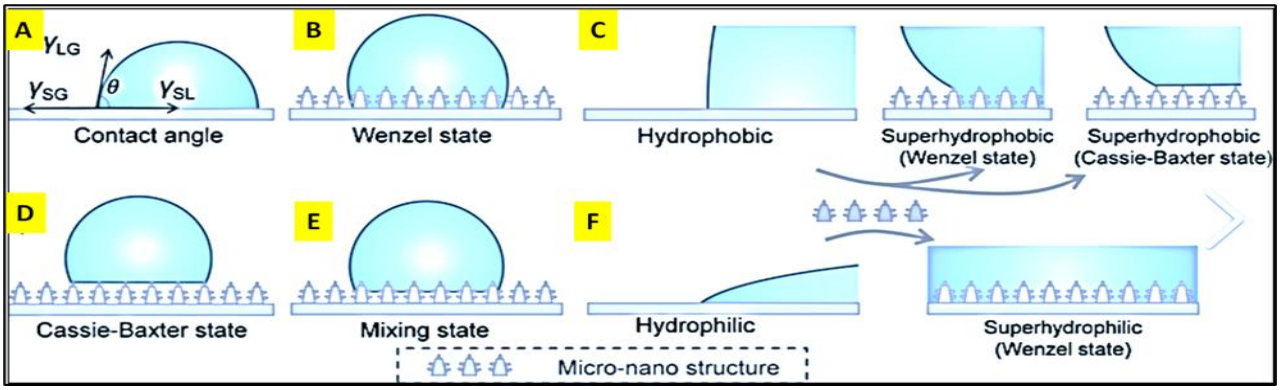

Figure 9. illustrates different liquid contact angles models.

3.2.5 Membrane thickness

Membrane thickness plays a vital role in MD membrane performance, with a direct effect on the transmission of heat and mass. A thinner membrane enhances permeate flow by decreasing the impedance of mass transfer, whereas a thicker membrane minimizes heat loss. This creates a trade-off between increased thermal efficiency and flux. However, in AGMD, the effect of membrane thickness on mass transfer is minimal, as the layer of stagnant air predominantly governs the mass transfer rate [139].

3.3. Conditions of the MD process

For optimal outcomes, the impact of several operational factors on MD performance needs to be managed. The following are some of these parameters: (i) length of operation; (ii) concentration of feed; (iii) kind of membrane; (iv) temperature of feed; and (v) length of operation.

3.3.1. Feed temperature

A major factor influencing permeate flux is feed temperature. The Antoine equation states that vapor pressure rises with temperature in an exponential fashion, leading to a corresponding exponential rise in permeate flux [143]. Because pressure of vapor is more delicate to higher temperatures, increasing the temperature of feed improves distillate flow while the temperature differential between the feed side and the permeate is maintained. Stated differently, the rise in vapor pressure gradient due to rising temperature of feed outweighs the influence of decreasing permeate-side gradient temperature. Additionally, studies have shown that raising the feed and permeate's temperature differential sides positively impacts the diffusion factor [144-145].

3.3.2. Feed solution concentration

A notable rise in feed solution concentration reduces permeate productivity due to a rising temperature polarization and falling vapor pressure. Studies have shown that raising the NaCl concentration from 0 to 2 mol resulted in approximately a 12% decline in permeate flux [146]. This reduction is primarily caused by the decrease in vapor pressure induced by higher solute concentrations. Additionally, researchers have identified three key factors contributing to flux decline with lowering water activity, (i) raising feed concentration, (ii) concentration polarization-induced reduce the mass transfer coefficient, and (iii) a reduction of the heat transfer coefficient brought on by a dip in temperature of the surface of membrane [147].

3.3.3. Membrane type

As previously mentioned, membranes of MD ought to have a high average pore size and a porous surface. The size and porosity of surface pores closely correlate with distillate flux, despite the fact that it is inversely related to pore tortuosity and membrane thickness. Additionally, membranes must exhibit a high LEP to prevent wetting. Studies have also shown that membranes which are not supported with a given pore volume achieve higher productivity compared to membranes that are supported and have same pore sizes [148].

3.3.4. Flow rate of feed current

The impact of feed current velocity on SGMD is minimal, whereas it plays an important part in (DCMD) and (VMD). Generally, increasing the distillate flux is improved by feed flow velocity due to better mixing and a thinner boundary layer on the membrane's feed side for temperature. As the flow rate of feed solution increases, the flow transitions from a laminar to a turbulent regime, eventually leading to an asymptotic distillate flux [149]. This increase in feed flow rate also raises the heat polarization by decreasing the heat transfer coefficient and Reynolds number.

3.3.5. Long-Term operation

Membrane's MD must maintain consistent performance over extended periods, ranging from days to months. In fact, membrane Stability continues to be a major obstacle. in MD commercialization. Several studies have shown that after an initial membrane compaction phase; permeate flux increases during the first few hours of operation [150-152]. However, over time the flux gradually declines until reaching a steady state. This reduction is primarily attributed to partial pore wetting and membrane fouling during long-term MD experiments [147].

3.4. Polymeric membranes for MD

Polymeric membranes often utilize in MD include, PVDF, PTFE, PP, and PE. PTFE and PVDF are preferred because of their great heat stability and hydrophobicity [153]. Adnan et al. investigated the effect of PTFE microstructure on water flux, finding that high porosity (62–82%) enhances water diffusion, while excessive thickness reduction leads to water-logging [154]. Shirazi et al. emphasized that uniform pore size distribution is crucial for performance, as demonstrated in a comparison of commercial PTFE membranes [155]. Li et al. used electrospinning to create a PVDF/PTFE composite membrane with a hydrophilic chitosan-polyethylene oxide layer [156]. While this structure slightly increased flux (from 15 to 19 L/m²/h), wetting caused performance decline over time. PVDF is notable for its ability to form asymmetric membranes via non-solvent induced phase separation method (NIPS). Hou et al. developed membranes of PVDF with hydrophobic $CaCO_3$ nanoparticles, improving water flux and thermal efficiency due to increased surface roughness and larger pore size [157]. A cost analysis by Macedonio et al. found that PVDF is more cost-effective than PP for MD desalination, owing to its higher water flux and lower heat loss [158]. Gryta .investigated PP membranes produced by method known as thermal-induced phase separation method (TIPS) and discovered that optimizing porosity for surface and reducing pore size (1–3 μm) mitigates membrane wetting [159]. Zuo et al. studied commercial PE membranes and discovered that larger pores led to reduction in heat dissipation and superior water flux compared to PTFE, PVDF, and PP, highlighting the role of pore interconnectivity [160].

3.4.1. Hydrophobic polymeric membrane fabrication for MD

Many approaches may be utilized to make synthetic membranes, and some of these processes can be employed to construct both ceramic and polymeric membranes. Numerous techniques have been described in the literature for creating hydrophobic polymeric membranes, including post-treatment, modification, and direct selection of the suitable hydrophobic polymer as starting materials [161]. As previously stated, in order to prevent certain molecules from escaping through the membrane barrier, membrane surfaces need possess unique properties. This characteristic, which prevents surface wettability, is called hydrophobicity or the "H2O repellent" trait. In essence, H2O interaction with hydrophobic surfaces tends to be decreased since spreading of H2O on these surfaces is impossible. Low surface energy causes spherical water droplets to form on hydrophobic surfaces [162]. One of the key factors in creating a hydrophobic surface is the chemistry of the surface molecules. When a surface bearing hydroxyl groups comes into touch with water, it usually becomes hydrophilic. The four hydrophobic polymers that have been studied the most for MD applications are PP, PTFE, PE, and PVDF. Hydrophobic membranes are preferred in MD because they can stop saline feed from getting into the membrane's pores (a process known as membrane wetting). For MD applications, symmetric membranes composed of PTFE and PP have been used [163, 164]. Since these membranes are insoluble in conventional solvents at room temperature, they are made by stretching and using heat. These symmetric membranes, which frequently have large holes, are very hydrophobic, yet they are unable to stop wetting with prolonged use. The fact that PVDF dissolves in common organic solvents is one of the primary factors contributing to its widespread use among the other polymers described above [165]. A few characteristics of membrane polymeric materials are displayed in Table 3.

Table 2: Characterization of selected polymeric membrane properties at 20 °C [166].

Membrane material	Surface energy (mN/m)	Thermal conductivity (Wm-1 K-1)	Thermal stability	Chemical stability
Polyethylene (PE)	33.2	28–33	Poor	Good
Polyethersulfone (PES)	113.7			
Polyvinylidenefluoride (PVDF)	30.3	0.19	Moderate	Good
Polyvinylidenefluoride (PVDF)	30.3	0.19	Moderate	Good
Polyvinylidene chloride (PVDC)	45.0	–	–	–
Polypropylene (PP)	30.0	0.17	Moderate	Good
Polyethyleneterephthalate (PET)	44.6	–	–	–
Polysulfone (PSF)	41.0	–	–	–
Polytetrafluoroethylene (PTFE)	19.1	0.25	Good	Good
Polyamide (PA)	35.9	–	–	–
Poly(dimethylsiloxane) (PDMS)	22.0	–	–	–

3.5. MD inorganic membranes

Inorganic membranes offer greater stability in terms of chemical, mechanical, and thermal properties than polymeric membranes, though their use in MD remains limited. Common types include ceramic, glass, and metallic membranes. Ceramic membranes, primarily made from aluminum oxide and zirconium oxide, are fabricated using sol-gel processes. Metal membranes, produced by sintering metal powders like tungsten and molybdenum, have received little attention. Glass membranes, composed of silicon oxide, are prepared using leaching or sol-gel techniques [173]

3.6. Mixed-matrix membranes for MD

To improve membrane performance in MD, mixed-matrix membranes (MMMs) blend inorganic materials with organic polymers. The selection of these materials is crucial, as it affects morphology and separation efficiency. Highly selective polymers improve separation, while the inorganic phase enhances thermal and chemical stability [174]. MMMs offer the structural stability of ceramics and the fabrication ease of polymers, making them a promising alternative [175]. These membranes are increasingly studied for water purification due to their balanced properties.

3.7. Photothermal membranes for MD Developments

Photothermal MD has drawn a lot of interest as an energy-efficient strategy for water desalination. Various composite membranes have been developed to enhance photothermal performance, including carbon black (CB)-based membranes as CB/PVDF [176], plasmonic gold nanoparticle (Au NPs)-incorporated membranes as Au/PVDF [26], and multi-walled carbon nanotubes (MWCNTs) as PSF/MWCNTs [131]…etc. These advanced

membranes improve light absorption, heat localization, and vapor transport, leading to enhanced water flux and thermal efficiency.

Two promising strategies in this field involve the use of noble-metal nanoparticles and carbon-based nanomaterials. Plasmonic photothermal MD utilizes noble-metal NPs to enhance water desalination efficiency by embedding Ag NPs into (PVDF) membranes as shown in Fig 10a. LSPR in Ag NPs generates nanoscale thermal hotspots, improving water evaporation rates. The study demonstrates that Ag NPs-loaded membranes significantly reduce temperature polarization, increase transmembrane flux, and achieve up to 11-fold higher vapor flux under UV irradiation compared to unloaded PVDF membranes through photothermal VMD system as illustrated in Fig 5. [177].

Another approach involves integrating MWCNTs into PSF matrix to enhance photothermal properties [131]. These composite membranes exhibit improved hydrophobicity, increased thermal stability, and efficient light-to-heat conversion as depicted in Fig 5c. when tested in a PMD system, they achieve higher water flux and improved thermal efficiency under both artificial and natural sunlight. The presence of MWCNTs enhances heat absorption and transfer, mitigating thermal polarization and facilitating vapor transport as significant in Fig 5d. These findings confirm the potential of both Ag NPs and MWCNTs-based membranes as promising advancements for energy-efficient MD applications.

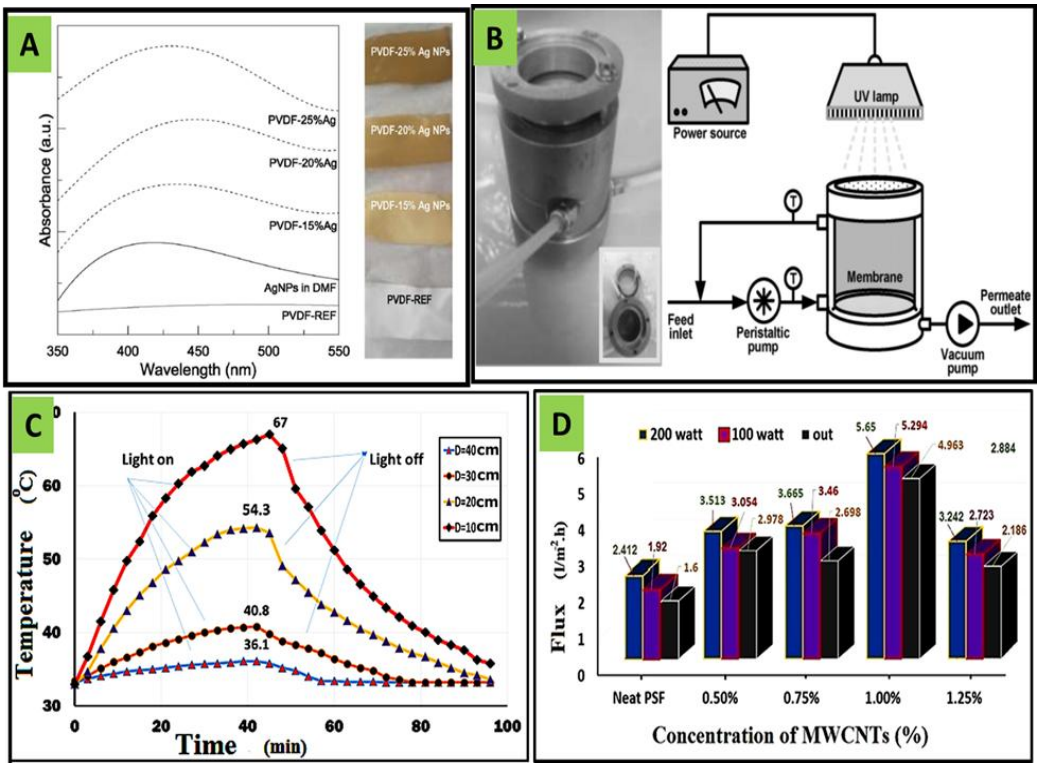

Figure 10: illustrates (a) UV Spectra of PVDF/Ag membranes with different Ag NPs concentrations (b) Photothermal VMD system. Reproduced with permission from [177]. Copyright Advanced materials, (c) Influence of light source displacement on PSF/MWCNTs membranes surface temperatures (d) Impact of various concentrations of MWCNTs on PMD flux of PSF membranes. Reproduced with permission from [131]. Copyright 2024 Iranian Polymer Journal.

4. Conclusion

In conclusion, we have provided an in-depth analysis of the recent advancement in MD which has become a promising method for treating water, offering energy-efficient, low-fouling, and low-pressure operation while utilizing renewable energy sources. Recent advances in photothermal membranes incorporating nanomaterials such as SiO_2/Au nanoshells, carbon black, and silver nanoparticles have significantly improved MD performance under solar irradiation. Parallel progress in nanotechnology has made it possible to create photothermal materials that effectively produce heat from NIR light, finding applications in water purification, bacterial disinfection, and cancer therapy. These materials fall into four major classes: semiconductors, carbon-based nanomaterials, plasmonic metals, and polymers. Each class presents unique mechanisms, such as LSPR in metals, electron–hole pair dynamics in semiconductors, also π–π* transitions in organic materials. Semiconductors like copper sulfides and carbon materials like graphene and CNTs have demonstrated outstanding solar vapor generation. Additionally, conjugated polymers and hybrid frameworks such as COFs and MOFs show great potential due to their high stability and light absorption capacity. Together, these advancements represent an exciting path forward for

scalable, sustainable, and multifunctional water purification systems in off-grid and resource-limited environments. As research continues to explore new materials and optimize existing ones, it is clear that photothermal nanocomposites will be essential to the future generation of technologies**.** Their integration into membrane distillation systems, particularly in solar-powered desalination, could revolutionize water purification processes, offering energy-efficient**,** economical, eco-friendly ways to fulfill the world's water needs. To fully realize the promise of these novel materials, further research should concentrate on resolving issues including membrane fouling, scalability, and long-term stability.

References

[1] Prinz, D. (2000, June). Global and European water challenges in the 21st Century. In Keynote Speech, 3rd Inter-Regional Conference on Environment-Water, “Water Resources Management in the 21st Century (pp. 1-3).

[2] Lu, K. J., & Chung, T. S. (2019). Introduction to Membrane Distillation. In Membrane Distillation (pp. 3-14). CRC Press.

[3] Sergio, Santoro., Ahmet, H., Avci., Antonio, Politano., Efrem, Curcio. (2022). The advent of thermoplasmonic membrane distillation.. Chemical Society Reviews, 51(14):6087-6125. Doi: 10.1039/d0cs00097.

[4] Adewole, J. K., Al Maawali, H. M., Jafary, T., Firouzi, A., & Oladipo, H. (2022). A review of seawater desalination with membrane distillation: material development and energy requirements. Water Supply, 22(12), 8500-8526.

[5] Cabassud, C., & Wirth, D. (2003). Membrane distillation for water desalination: how to choose an appropriate membrane?. Desalination, 157(1-3), 307-314.

[6] Maab, H., Francis, L., Al-Saadi, A., Aubry, C., Ghaffour, N., Amy, G., & Nunes, S. P. (2012). Synthesis and fabrication of nanostructured hydrophobic polyazole membranes for low-energy water recovery. Journal of Membrane Science, 423, 11-19.

[7] Adham, S., Hussain, A., Matar, J. M., Dores, R., & Janson, A. (2013). Application of membrane distillation for desalting brines from thermal desalination plants. Desalination, 314, 101-108.

[8] Meindersma, G. W., Guijt, C. M., & De Haan, A. B. (2006). Desalination and water recycling by air gap membrane distillation. Desalination, 187(1-3), 291-301.

[9] Al-Obaidani, S., Curcio, E., Macedonio, F., Di Profio, G., Al-Hinai, H., & Drioli, E. (2008). Potential of membrane distillation in seawater desalination: thermal efficiency, sensitivity study and cost estimation. Journal of membrane science, 323(1), 85-98.

[10] El Amali, A., Bouguecha, S., & Maalej, M. (2004). Experimental study of air gap and direct contact membrane distillation configurations: application to geothermal and seawater desalination. Desalination , 168, 357.

[11] Li, N. N., Fane, A. G., Ho, W. W., & Matsuura, T. (Eds.). (2011). Advanced membrane technology and applications. John Wiley & Sons.

[12] Lawson, K. W., & Lloyd, D. R. (1997). Membrane distillation. Journal of membrane Science, 124(1), 1-25.

[13] Sudoh, M., Takuwa, K., Iizuka, H., & Nagamatsuya, K. (1997). Effects of thermal and concentration boundary layers on vapor permeation in membrane distillation of aqueous lithium bromide solution. Journal of membrane science, 131(1-2), 1-7.

[14] Martínez, L., Florido-Díaz, F. J., Hernández, A., & Prádanos, P. (2002). Characterisation of three hydrophobic porous membranes used in membrane distillation: Modelling and evaluation of their water vapour permeabilities. Journal of membrane science, 203(1-2), 15-27.

[15] Schofield, R. W., Fane, A. G., & Fell, C. J. D. (1990). Gas and vapour transport through microporous membranes. I. Knudsen-Poiseuille transition. Journal of Membrane Science, 53(1-2), 159-171.

[16] Gebhart, B. (1993). Heat conduction and mass diffusion. (No Title).

[17] Gryta, M., & Tomaszewska, M. (1998). Heat transport in the membrane distillation process. Journal of membrane science, 144(1-2), 211-222.

[18] Alkhudhiri, A., Darwish, N., & Hilal, N. (2012). Membrane distillation: A comprehensive review. Desalination, 287, 2-18.

[19] El-Bourawi, M. S., Khayet, M., Ma, R., Ding, Z., Li, Z., & Zhang, X. (2007). Application of vacuum membrane distillation for ammonia removal. Journal of Membrane Science, 301(1-2), 200-209.

[20] Fahmey, M. S., El-Aassar, A. H. M., Abo-Elfadel, M. M., Orabi, A. S., & Das, R. (2019). Comparative performance evaluations of nanomaterials mixed polysulfone: A scale-up approach through vacuum enhanced direct contact membrane distillation for water desalination. Desalination, 451, 111-116.

[21] Politano, A., Al-Juboori, R. A., Alnajdi, S., Alsaati, A., Athanassiou, A., Bar-Sadan, M., ... & Curcio, E. (2024). 2024 roadmap on membrane desalination technology at the water-energy nexus. Journal of Physics: Energy, 6(2), 021502.

[22] Costa, F. C., Fortes, A. R., Braga, C. D., Arcanjo, G. S., Grossi, L., Mounteer, A. H., ... & Amaral, M. C. (2022). Assessment of a hybrid UV-LED-membrane distillation process: Focus on fouling mitigation. Separation and Purification Technology, 292, 121003.

[23] Tong, T., & Elimelech, M. (2016). The global rise of zero liquid discharge for wastewater management: drivers, technologies, and future directions. Environmental science & technology, 50(13), 6846-6855.

[24] Kalogirou, S. A. (2004). Solar thermal collectors and applications. Progress in energy and combustion science, 30(3), 231-295.

[25] Schofield, R. W., Fane, A. G., & Fell, C. J. D. (1987). Heat and mass transfer in membrane distillation. Journal of membrane Science, 33(3), 299-313.

[26] Wu, Jinjian, et al. "Photothermal nanocomposite membranes for direct solar membrane distillation." Journal of Materials Chemistry A 5.45 (2017): 23712-23719.

[27] Wang, Y., Wei, T., Wang, Y., Zeng, J., Wang, T., Wang, Q., ... & Wang, X. (2024). Quasi-waffle solar distiller for durable desalination of seawater. Science Advances, 10(22), eadk1113.

[28] Dongare, P. D., Alabastri, A., Pedersen, S., Zodrow, K. R., Hogan, N. J., Neumann, O., ... & Halas, N. J. (2017). Nanophotonics-enabled solar membrane distillation for off-grid water purification. Proceedings of the National Academy of Sciences, 114(27), 6936-6941.

[29] Politano, A., Argurio, P., Di Profio, G., Sanna, V., Cupolillo, A., Chakraborty, S., ... & Curcio, E. (2017). Photothermal membrane distillation for seawater desalination. Advanced materials, 29(2), 1603504.

[30] Mohammadi, T., & Akbarabadi, M. (2005). Separation of ethylene glycol solution by vacuum membrane distillation (VMD). Desalination, 181(1-3), 35-41.

[31] Findley, M. E. (1967). Vaporization through porous membranes. Industrial & Engineering Chemistry Process Design and Development, 6(2), 226-230.

[32] Ding, Z., Ma, R., & Fane, A. G. (2003). A new model for mass transfer in direct contact membrane distillation. Desalination, 151(3), 217-227.

[33] Tee, S. Y., Win, K. Y., Goh, S. S., Teng, C. P., Tang, K. Y., Regulacio, M. D., ... & Ye, E. (2022). Introduction to photothermal nanomaterials.

[34] Liang, J., Liu, H., Yu, J., Zhou, L., & Zhu, J. (2019). Plasmon-enhanced solar vapor generation. Nanophotonics, 8(5), 771-786.

[35] Furube, A., & Hashimoto, S. (2017). Insight into plasmonic hot-electron transfer and plasmon molecular drive: new dimensions in energy conversion and nanofabrication. NPG Asia Materials, 9(12), e454-e454.

[36] Yu, H., Peng, Y., Yang, Y., & Li, Z. Y. (2019). Plasmon-enhanced light–matter interactions and applications. npj Computational Materials, 5(1), 45.

[37] Webb, J. A., & Bardhan, R. (2014). Emerging advances in nanomedicine with engineered gold nanostructures. Nanoscale, 6(5), 2502-2530.

[38] Link, S., & El-Sayed, M. A. (1999). Spectral properties and relaxation dynamics of surface plasmon electronic oscillations in gold and silver nanodots and nanorods. The Journal of Physical Chemistry B, 103(40), 8410-8426.

[39] Link, S., & El-Sayed, M. A. (2000). Shape and size dependence of radiative, non-radiative and photothermal properties of gold nanocrystals. International reviews in physical chemistry, 19(3), 409-453.

[40] Hu, M., Chen, J., Li, Z. Y., Au, L., Hartland, G. V., Li, X., ... & Xia, Y. (2006). Gold nanostructures: engineering their plasmonic properties for biomedical applications. Chemical Society Reviews, 35(11), 1084-1094.

[41] Motl, N. E., Ewusi-Annan, E., Sines, I. T., Jensen, L., & Schaak, R. E. (2010). Au− Cu alloy nanoparticles with tunable compositions and plasmonic properties: Experimental determination of composition and correlation with theory. The Journal of Physical Chemistry C, 114(45), 19263-19269.

[42] Lalisse, A., Tessier, G., Plain, J., & Baffou, G. (2015). Quantifying the efficiency of plasmonic materials for near-field enhancement and photothermal conversion. The Journal of Physical Chemistry C, 119(45), 25518-25528.

[43] Zhou, L., Tan, Y., Wang, J., Xu, W., Yuan, Y., Cai, W., & Zhu, J. (2016). 3D self-assembly of aluminum nanoparticles for plasmon-enhanced solar desalination. Nature photonics, 10(6), 393-398.

[44] Pujari, A., & Thomas, T. (2020). Al–Cu core-shell nanoparticles as an alternative to noble metal plasmonics: A computational study. Materials Chemistry and Physics, 253, 123419.

[45] Manthiram, K., & Alivisatos, A. P. (2012). Tunable localized surface plasmon resonances in tungsten oxide nanocrystals. Journal of the American Chemical Society, 134(9), 3995-3998.

[46] Liang, H., Xi, H., Liu, S., Zhang, X., & Liu, H. (2019). Modulation of oxygen vacancy in tungsten oxide nanosheets for Vis-NIR light-enhanced electrocatalytic hydrogen production and anticancer photothermal therapy. Nanoscale, 11(39), 18183-18190.

[47] Li, B., Wang, X., Wu, X., He, G., Xu, R., Lu, X., & Parkin, I. P. (2017). Phase and morphological control of MoO_{3-x} nanostructures for efficient cancer theragnosis therapy . Nanoscale, 9(31), 11012-11016.

[48] Ge, S., Wong, K. W., & Ng, K. M. (2017). Revitalizing digenite Cu 1.8 S nanoparticles with the localized surface plasmon resonance (LSPR) effect by manganese incorporation. New Journal of Chemistry, 41(2), 677-684.

[49] Hessel, C. M., Pattani, V. P., Rasch, M., Panthani, M. G., Koo, B., Tunnell, J. W., & Korgel, B. A. (2011). Copper selenide nanocrystals for photothermal therapy. Nano letters, 11(6), 2560-2566.

[50] Zhao, Y. D., Han, J., Chen, Y., Su, Y., Cao, Y. M., Wu, B... & Liao, L. S. (2022). Organic charge-transfer cocrystals toward large-area nanofiber membrane for photothermal conversion and imaging. ACS nano, 16(9), 15000-15007.

[51] Boca, S. C., Potara, M., Gabudean, A. M., Juhem, A., Baldeck, P. L., & Astilean, S. (2011). Chitosan-coated triangular silver nanoparticles as a novel class of biocompatible, highly effective photothermal transducers for in vitro cancer cell therapy. Cancer letters, 311(2), 131-140.

[52] Boca-Farcau, S., Potara, M., Simon, T., Juhem, A., Baldeck, P., & Astilean, S. (2014). Folic acid-conjugated, SERS-labeled silver nanotriangles for multimodal detection and targeted photothermal treatment on human ovarian cancer cells. Molecular pharmaceutics, 11(2), 391-399.

[53] D'Agostino, A., Taglietti, A., Grisoli, P., Dacarro, G., Cucca, L., Patrini, M., & Pallavicini, P. (2016). Seed mediated growth of silver nanoplates on glass: Exploiting the bimodal antibacterial effect by near IR photo-thermal action and Ag+ release. RSC Advances, 6(74), 70414-70423.

[54] D'Agostino, A., Taglietti, A., Desando, R., Bini, M., Patrini, M., Dacarro, G., & Grisoli, P. (2017). Bulk surfaces coated with triangular silver nanoplates: Antibacterial action based on silver release and photo-thermal effect. Nanomaterials, 7(1), 7.

[55] Botteon, C. E. A., Silva, L. B., Ccana-Ccapatinta, G. V., Silva, T. S., Ambrosio, S. R., Veneziani, R. C. S., ... & Marcato, P. D. (2021). Biosynthesis and characterization of gold nanoparticles using Brazilian red propolis and evaluation of its antimicrobial and anticancer activities. Scientific Reports, 11(1), 1974.

[56] Regulacio, M. D., Yang, D. P., & Ye, E. (2020). Toward greener methods of producing branched metal nanostructures. CrystEngComm, 22(3), 399-411.

[57] Yang, D. P., Liu, X., Teng, C. P., Owh, C., Win, K. Y., Lin, M. ... & Ye, E. (2017). Unexpected formation of gold nanoflowers by a green synthesis method as agents for a safe and effective photothermal therapy. Nanoscale, 9(41), 15753-15759.

[58] Addissouky, T. A., El Sayed, I. E. T., Ali, M. M., Alubiady, M. H. S., & Wang, Y. (2024). Precision medicine and immunotherapy advances transforming colorectal cancer treatment. Journal of Cancer Biology, 5(2), 38-43.

[59] Chen, X., Liu, L., & Huang, F. (2015). Black titanium dioxide (TiO 2) nanomaterials. Chemical Society Reviews, 44(7), 1861-1885.

[60] Xu, D., Mao, J., He, Y., & Yeung, E. S. (2014). Size-tunable synthesis of high-quality gold nanorods under basic conditions by using H 2 O 2 as the reducing agent. Journal of Materials Chemistry C, 2(25), 4989-4996.

[61] Liao, J., Li, W., Peng, J., Yang, Q., Li, H., Wei, Y., & Qian, Z. (2015). Combined cancer photothermal-chemotherapy based on doxorubicin/gold nanorod-loaded polymers-omes. Theranostics, 5(4), 345.

[62] Zhang, Q., Wang, L., Jiang, Y., Gao, W., Wang, Y., Yang, X. ... & Liu, Z. (2017). Gold nanorods with silica shell and PAMAM

dendrimers for efficient photothermal therapy and low toxic codelivery of anticancer drug and siRNA. Advanced Materials Interfaces, 4(24), 1701166.

[63] Xu, W., Qian, J., Hou, G., Suo, A., Wang, Y., Wang, J., ... & Yao, Y. (2017). Hyaluronic acid-functionalized gold nanorods with pH/NIR dual-responsive drug release for synergetic targeted photothermal chemotherapy of breast cancer. ACS applied materials & interfaces, 9(42), 36533-36547.

[64] Wang, S., Lin, Q., Xu, W., An, Q., Zhou, R., Yu, C. J., ... & Yuan, Z. (2020). Precisely tuning the longitudinal localized surface plasmon resonance of gold nanorods via additive-regulated overgrowth. RSC advances, 10(21), 12619-12625.

[65] Tee, Si Yin, Enyi Ye, Choon Peng Teng, Yuki Tanaka, Karen Yuanting Tang, Khin Yin Win, and Ming-Yong Han. "Advances in photothermal nanomaterials for biomedical, environmental and energy applications." Nanoscale 13, no. 34 (2021): 14268-14286.

[66] Huang, X., & El-Sayed, M. A. (2010). Gold nanoparticles: Optical properties and implementations in cancer diagnosis and photothermal therapy. Journal of advanced research, 1(1), 13-28.

[67] Tian, Q., Hu, J., Zhu, Y., Zou, R., Chen, Z., Yang, S. ... & Liu, X. (2013). Sub-10 nm Fe3O4@ $Cu_{2-x}S$ core–shell nanoparticles for dual-modal imaging and photothermal therapy. Journal of the American Chemical Society, 135(23), 8571-8577.

[68] Wu, X., Chen, G. Y., Owens, G., Chu, D., & Xu, H. (2019). Photothermal materials: A key platform enabling highly efficient water evaporation driven by solar energy. Materials Today Energy, 12, 277-296.

[69] Orendorff, C. J., & Murphy, C. J. (2006). Quantitation of metal content in the silver-assisted growth of gold nanorods. The Journal of Physical Chemistry B, 110(9), 3990-3994.

[70] Huang, X., Tang, S., Mu, X., Dai, Y., Chen, G., Zhou, Z. ... & Zheng, N. (2011). Freestanding palladium nanosheets with plasmonic and catalytic properties. Nature nanotechnology, 6(1), 28-32.

[71] Tang, S., Chen, M., & Zheng, N. (2014). Sub-10-nm Pd Nanosheets with renal clearance for efficient near-infrared photothermal cancer therapy. Small, 10(15), 3139-3144.

[72] Huang, X., Tang, S., Yang, J., Tan, Y., & Zheng, N. (2011). Etching growth under surface confinement: an effective strategy to prepare mesocrystalline Pd nanocorolla. Journal of the American Chemical Society, 133(40), 15946-15949.

[73] Xiao, J. W., Fan, S. X., Wang, F., Sun, L. D., Zheng, X. Y., & Yan, C. H. (2014). Porous Pd nanoparticles with high photothermal conversion efficiency for efficient ablation of cancer cells. Nanoscale, 6(8), 4345-4351.

[74] Wang, Y., Black, K. C., Luehmann, H., Li, W., Zhang, Y., Cai, X., & Xia, Y. (2013). ACS Nano, 2013, 7, 2068-2077. This article is licensed under a Creative Commons Attribution-Noncommercial, 3.

[75] Ye, E., Win, K. Y., Tan, H. R., Lin, M., Teng, C. P., Mlayah, A., & Han, M. Y. (2011). Plasmonic gold nanocrosses with multidirectional excitation and strong photothermal effect. Journal of the American Chemical Society, 133(22), 8506-8509.

[76] Ye, E., Regulacio, M. D., Bharathi, M. S., Pan, H., Lin, M., Bosman, M., & Han, M. Y. (2016). An experimental and theoretical investigation of the anisotropic branching in gold nanocrosses. Nanoscale, 8(1), 543-552.

[77] Huang, X., Jain, P. K., El-Sayed, I. H., & El-Sayed, M. A. (2006). Determination of the minimum temperature required for selective photothermal destruction of cancer cells with the use of immunotargeted gold nanoparticles. Photochemistry and photobiology, 82(2), 412-417.

[78] Panchapakesan, B., Book-Newell, B., Sethu, P., Rao, M., & Irudayaraj, J. (2011). Gold nanoprobes for theranostics. Nanomedicine, 6(10), 1787-1811.

[79] Cho, E. C., Kim, C., Zhou, F., Cobley, C. M., Song, K. H., Chen, J., & Xia, Y. (2009). Measuring the optical absorption cross sections of Au− Ag nanocages and au nanorods by photoacoustic imaging. The Journal of Physical Chemistry C, 113(21), 9023-9028.

[80] Yu, H., Peng, Y., Yang, Y., & Li, Z. Y. (2019). Plasmon-enhanced light–matter interactions and applications. npj Computational Materials, 5(1), 45.

[81] Ni, G., Miljkovic, N., Ghasemi, H., Huang, X., Boriskina, S. V., Lin, C. T., & Chen, G. (2015). Volumetric solar heating of nanofluids for direct vapor generation. Nano Energy, 17, 290-301.

[82] Gao, X., Ren, H., Zhou, J., Du, R., Yin, C., Liu, R. ... & Zhang, J. (2017). Synthesis of hierarchical graphdiyne-based architecture for efficient solar steam generation. Chemistry of Materials, 29(14), 5777-5781.

[83] Wang, Y., Zhang, L., & Wang, P. (2016). Self-floating carbon nanotube membrane on macroporous silica substrate for highly efficient solar-driven interfacial water evaporation. ACS Sustainable Chemistry & Engineering, 4(3), 1223-1230.

[84] Chen, C., Li, Y., Song, J., Yang, Z., Kuang, Y., Hitz, E. ... & Hu, L. (2017). Highly flexible and efficient solar steam generation device. Advanced materials, 29(30), 1701756.

[85] Li, X., Lin, R., Ni, G., Xu, N., Hu, X., Zhu, B., ... & Zhu, J. (2018). Three-dimensional artificial transpiration for efficient solar waste-water treatment. National Science Review, 5(1), 70-77.

[86] Shi, L., Wang, Y., Zhang, L., & Wang, P. (2017). Rational design of a bi-layered reduced graphene oxide film on polystyrene foam for solar-driven interfacial water evaporation. Journal of Materials Chemistry A, 5(31), 16212-16219.

[87] Yang, J., Pang, Y., Huang, W., Shaw, S. K., Schiffbauer, J., Pillers, M. A., ... & Luo, T. (2017). Functionalized graphene enables highly efficient solar thermal steam generation. ACS nano, 11(6), 5510-5518.

[88] Yang, Y., Zhao, R., Zhang, T., Zhao, K., Xiao, P., Ma, Y. ... & Chen, Y. (2018). Graphene-based standalone solar energy converter for water desalination and purification. ACS nano, 12(1), 829-835.

[89] Guo, A., Ming, X., Fu, Y., Wang, G., & Wang, X. (2017). Fiber-based, double-sided, reduced graphene oxide films for efficient solar vapor generation. ACS applied materials & interfaces, 9(35), 29958-29964.

[90] Dongare, P. D., Alabastri, A., Pedersen, S., Zodrow, K. R., Hogan, N. J., Neumann, O., ... & Halas, N. J. (2017). Nanophotonics-enabled solar membrane distillation for off-grid water purification. Proceedings of the National Academy of Sciences, 114(27), 6936-6941.

[91] Zhuang, S., Zhou, L., Xu, W., Xu, N., Hu, X., Li, X. ... & Zhu, J. (2018). Tuning transpiration by interfacial solar absorber-leaf engineering. Advanced Science, 5(2), 1700497.

[92] Geng, J., Sun, C., Liu, J., Liao, L. D., Yuan, Y., Thakor, N. ... & Liu, B. (2015). Biocompatible conjugated polymer nanoparticles for efficient photothermal tumor therapy. Small, 11(13), 1603-1610.

[93] Guo, B., Feng, G., Manghnani, P. N., Cai, X., Liu, J., Wu, W., ... & Liu, B. (2016). A porphyrin-based conjugated polymer for highly efficient in vitro and in vivo photothermal therapy. Small, 12(45), 6243-6254.

[94] Chen, P., Ma, Y., Zheng, Z., Wu, C., Wang, Y., & Liang, G. (2019). Facile syntheses of conjugated polymers for photothermal tumour therapy. Nature communications, 10(1), 1192.

[95] Yu, C., Xu, L., Zhang, Y., Timashev, P. S., Huang, Y., & Liang, X. J. (2020). Polymer-based nanomaterials for noninvasive cancer photothermal therapy. ACS Applied Polymer Materials, 2(10), 4289-4305.

[96] Waller, P. J., Gándara, F., & Yaghi, O. M. (2015). Chemistry of covalent organic frameworks. Accounts of chemical research, 48(12), 3053-3063.

[97] Bessinger, D., Ascherl, L., Auras, F., & Bein, T. (2017). Spectrally switchable photodetection with near-infrared-absorbing covalent organic frameworks. Journal of the American Chemical Society, 139(34), 12035-12042.

[98] Smith, B. J., Overholts, A. C., Hwang, N., & Dichtel, W. R. (2016). Insight into the crystallization of amorphous imine-linked polymer networks to 2D covalent organic frameworks. Chemical Communications, 52(18), 3690-3693.

[99] Tan, J., Namuangruk, S., Kong, W., Kungwan, N., Guo, J., & Wang, C. (2016). Manipulation of amorphous-to-crystalline transformation: Towards the construction of covalent organic framework hybrid microspheres with NIR photothermal conversion ability. Angewandte Chemie International Edition, 55(45), 13979-13984.

[100] Hu, C., Zhang, Z., Liu, S., Liu, X., & Pang, M. (2019). Monodispersed CuSe sensitized covalent organic framework photosensitizer with an enhanced photodynamic and photothermal effect for cancer therapy. ACS applied materials & interfaces, 11(26), 23072-23082.

[101] Espín, J., Garzón-Tovar, L., Boix, G., Imaz, I., & Maspoch, D. (2018). The photothermal effect in MOFs: covalent post-synthetic modification of MOFs mediated by UV-Vis light under solvent-free conditions. Chemical Communications, 54(33), 4184-4187.

[102] Espín, J., Garzón-Tovar, L., Carné-Sánchez, A., Imaz, I., & Maspoch, D. (2018). Photothermal activation of metal–organic frameworks using a UV–vis light source. ACS applied materials & interfaces, 10(11), 9555-9562.

[103] Wang, W., Wang, L., Li, Y., Liu, S., Xie, Z., & Jing, X. (2016). Nanoscale polymer metal–organic framework hybrids for effective photothermal therapy of colon cancers. Advanced Materials, 28(42), 9320-9325.

[104] Alkhudhiri, A., Darwish, N., & Hilal, N. (2012). Membrane distillation: A comprehensive review. Desalination, 287, 2-18.

[105] Drioli, E., Ali, A., & Macedonio, F. (2015). Membrane distillation: Recent developments and perspectives. Desalination, 356, 56-84.

[106] Khayet, M. (2011). Membranes and theoretical modeling of membrane distillation: A review. Advances in colloid and interface science, 164(1-2), 56-88.

[107] García-Payo, M. D. C., Essalhi, M., & Khayet, M. (2010). Effects of PVDF-HFP concentration on membrane distillation performance and structural morphology of hollow fiber membranes. Journal of Membrane Science, 347(1-2), 209-219.

[108] Hou, D., Wang, J., Sun, X., Ji, Z., & Luan, Z. (2012). Preparation and properties of PVDF composite hollow fiber membranes for desalination through direct contact membrane distillation. Journal of membrane science, 405, 185-200.

[109] Feng, C., Khulbe, K. C., Matsuura, T., Gopal, R., Kaur, S., Ramakrishna, S., & Khayet, M. (2008). Production of drinking water from saline water by air-gap membrane distillation using polyvinylidene fluoride nanofiber membrane. Journal of Membrane Science, 311(1-2), 1-6.

[110] Mengual, J. I., Khayet, M., & Godino, M. P. (2004). Heat and mass transfer in vacuum membrane distillation. International Journal of Heat and Mass Transfer, 47(4), 865-875.

[111] Wu, B., Tan, X., Li, K., & Teo, W. K. (2006). Removal of 1, 1, 1-trichloroethane from water using a polyvinylidene fluoride hollow fiber membrane module: Vacuum membrane distillation operation. Separation and Purification Technology, 52(2), 301-309.

[112] Zhao, Z. P., Ma, F. W., Liu, W. F., & Liu, D. Z. (2008). Concentration of ginseng extracts aqueous solution by vacuum membrane distillation. 1. Effects of operating conditions. Desalination, 234(1-3), 152-157.

[113] Safavi, M., & Mohammadi, T. (2009). High-salinity water desalination using VMD. Chemical Engineering Journal, 149(1-3), 191-195.

[114] Mericq, J. P., Laborie, S., & Cabassud, C. (2010). Vacuum membrane distillation of seawater reverse osmosis brines. Water research, 44(18), 5260-5273.

[115] El-Bourawi, M. S., Ding, Z., Ma, R., & Khayet, M. (2006). A framework for better understanding membrane distillation separation process. Journal of membrane science, 285(1-2), 4-29.

[116] Curcio, E., & Drioli, E. (2005). Membrane distillation and related operations—a review. Separation and Purification Reviews, 34(1), 35-86.

[117] Banat, F., Al-Rub, F. A., & Bani-Melhem, K. (2003). Desalination by vacuum membrane distillation: sensitivity analysis. *Separation and Purification Technology*, *33*(1), 75-87.

[118] Singh, D., & Sirkar, K. K. (2012). Desalination by air gap membrane distillation using a two hollow-fiber-set membrane module. Journal of membrane science, 421, 172-179.

[119] Khayet, M., & Matsuura, T. (2011). Membrane distillation (Vol. 41, chapter1, page 3). Amsterdam: Elsevier.

[120] Cath, T. Y., Adams, V. D., & Childress, A. E. (2004). Experimental study of desalination using direct contact membrane distillation: a new approach to flux enhancement. Journal of Membrane Science, 228(1), 5-16.

[121] Rao, G., Hiibel, S. R., Achilli, A., & Childress, A. E. (2015). Factors contributing to flux improvement in vacuum-enhanced direct contact membrane distillation. Desalination, 367, 197-205.

[122] Naidu, G., Jeong, S., Vigneswaran, S., Jang, E. K., Choi, Y. J., & Hwang, T. M. (2016). Fouling study on vacuum-enhanced direct contact membrane distillation for seawater desalination. Desalination and Water Treatment, 57(22), 10042-10051.

[123] Francis, L., Ghaffour, N., Alsaadi, A. A., & Amy, G. L. (2013). Material gap membrane distillation: A new design for water vapor flux enhancement. Journal of membrane science, 448, 240-247.

[124] Zhao, K., Heinzl, W., Wenzel, M., Büttner, S., Bollen, F., Lange, G. ... & Sarda, N. (2013). Experimental study of the memsys vacuum-multi-effect-membrane-distillation (V-MEMD) module. Desalination, 323, 150-160.

[125] Taylor, C. R. (2018). Direct Contact Membrane Distillation for Solar Water Needs (Master's thesis, University of Nevada, Reno).

[126] Naidu, G., Jeong, S., Choi, Y., Jang, E., Hwang, T. M., & Vigneswaran, S. (2014). Application of vacuum membrane distillation for small scale drinking water production. Desalination, 354, 53-61.

[127] Heinzl, W., Büttner, S., & Lange, G. (2012). Industrialized modules for MED Desalination with polymer surfaces. Desalination and water treatment, 42(1-3), 177-180.

[128] Lee, J. G., & Kim, W. S. (2014). Numerical study on multi-stage vacuum membrane distillation with economic evaluation. Desalination, 339, 54-67.

[129] Li, X., Qin, Y., Liu, R., Zhang, Y., & Yao, K. (2012). Study on concentration of aqueous sulfuric acid solution by multiple-effect membrane distillation. Desalination, 307, 34-41.

[130] Chafidz, A., Kerme, E. D., Wazeer, I., Khalid, Y., Ajbar, A., & Al-Zahrani, S. M. (2016). Design and fabrication of a portable and hybrid solar-powered membrane distillation system. Journal of cleaner production, 133, 631-647.

[131] Hameed, A. M., Alayyafi, A. A., Alluhaybi, A. A., Fahmi, M. S., & Ali, M. E. (2024). Photothermal efficiency of carbon nanotubes-embedded polysulfone membranes for direct contact membrane distillation. Iranian Polymer Journal, 33(10), 1369-1380.

[132] Jang, E., Nam, S. H., Hwang, T. M., Lee, S., & Choi, Y. (2015). Effect of operating parameters on temperature and concentration polarization in vacuum membrane distillation process. Desalination and Water Treatment, 54(4-5), 871-880.

[133] Ugrozov, V. V., Elkina, I. B., Nikulin, V. N., & Kataeva, L. I. (2003). Theoretical and experimental research of liquid-gap membrane distillation process in membrane module. Desalination, 157(1-3), 325-331.

[134] Gryta, M., Karakulski, K., & Morawski, A. W. (2001). Purification of oily wastewater by hybrid UF/MD. Water research, 35(15), 3665-3669.

[135] Drioli, E., Lagana, F., Criscuoli, A., & Barbieri, G. (1999). Integrated membrane operations in desalination processes. Desalination, 122(2-3), 141-145.

[136] Gryta, M. (2001). The fermentation process integrated with membrane distillation. Separation and purification Technology, 24(1-2), 283-296.

[137] Khayet, M., Mengual, J. I., & Zakrzewska-Trznadel, G. (2006). Direct contact membrane distillation for nuclear desalination, Part II: experiments with radioactive solutions. International journal of nuclear desalination, 2(1), 56-73.

[138] Li, W., Chen, Y., Yao, L., Ren, X., Li, Y., & Deng, L. (2020). Fe3O4/PVDF-HFP photothermal membrane with in-situ heating for sustainable, stable and efficient pilot-scale solar-driven membrane distillation. *Desalination*, *478*, 114288.

[139] Kebria, M. R. S., & Rahimpour, A. (2020). Membrane distillation: basics, advances, and applications. Advances in membrane technologies.

[140] Franken, A. C. M., Nolten, J. A. M., Mulder, M. H. V., Bargeman, D., & Smolders, C. A. (1987). Wetting criteria for the applicability of membrane distillation. Journal of membrane science, 33(3), 315-328.

[141] Liao, Y., Wang, R., Tian, M., Qiu, C., & Fane, A. G. (2013). Fabrication of polyvinylidene fluoride (PVDF) nanofiber membranes by electro-spinning for direct contact membrane distillation. Journal of Membrane Science, 425, 30-39.

[142] Phattaranawik, J., Jiraratananon, R., & Fane, A. G. (2003). Heat transport and membrane distillation coefficients in direct contact membrane distillation. Journal of membrane science, 212(1-2), 177-193.

[143] Alklaibi, A. M., & Loir, N. (2005). Membrane-distillation desalination: status and potential. Desalination, 171(2), 111-131.

[144] Larimi, Y. N., Mollahosseini, A., Mohammadi, P., & Tabatabaei, M. (2016). Waste polymers recycling in biodiesel as a strategy to simultaneously enhance fuel properties and recycle the waste: Realistic simulation and economical assessment approach. Biofuels, 7(5), 559-570.

[145] Mollahosseini, A., & Abdelrasoul, A. (2019). Recent advances in thin film composites membranes for brackish groundwater treatment with critical focus on Saskatchewan water sources. Journal of Environmental Sciences, 81, 181-194.

[146] Qtaishat, M., Matsuura, T., Kruczek, B., & Khayet, M. (2008). Heat and mass transfer analysis in direct contact membrane distillation. Desalination, 219(1-3), 272-292.

[147] Lawson, K. W., & Lloyd, D. R. (1997). Membrane distillation. Journal of membrane Science, 124(1), 1-25.

[148] Izquierdo-Gil, M. A., Garcıa-Payo, M. C., & Fernandez-Pineda, C. (1999). Air gap membrane distillation of sucrose aqueous solutions. Journal of membrane science, 155(2), 291-307.

[149] Khayet, M., Godino, M. P., & Mengual, J. I. (2003). Possibility of nuclear desalination through various membrane distillation configurations: a comparative study. International journal of nuclear desalination, 1(1), 30-46.

[150] Banat, F. A., & Simandl, J. (1994). Theoretical and experimental study in membrane distillation. Desalination, 95(1), 39-52.

[151] Okiel, K., El-Aassar, A. H. M., Temraz, T., El-Etriby, S., & Shawky, H. A. (2016). Performance assessment of synthesized CNT/polypropylene composite membrane distillation for oil field produced water desalination. Desalination and Water Treatment, 57(24), 10995-11007.

[152] Drioli, E., & Wu, Y. (1985). Membrane distillation: an experimental study. Desalination, 53(1-3), 339-346.

[153] Rodgers, R., Hart, L., Hammerstein, O., & Sondheim, S. (1972). Richard Rodgers. Longines Symphonette Society.

[154] Adnan, S., Hayat Khan, A., Haider, S., & Mahmood, R. (2012). Solar energy potential in Pakistan. Journal of renewable and Sustainable Energy, 4(3).

[155] Shirazi, M. M. A., Kargari, A., & Tabatabaei, M. (2014). Evaluation of commercial PTFE membranes in desalination by direct contact membrane distillation. Chemical engineering and processing: Process intensification, 76, 16-25.

[156] Li, J., Ren, L. F., Shao, J., Tu, Y., Ma, Z., Lin, Y., & He, Y. (2020). Fabrication of triple layer composite membrane and its application in membrane distillation (MD): Effect of hydrophobic-hydrophilic membrane structure on MD performance. Separation and Purification Technology, 234, 116087.

[157] Hou, D., Wang, J., Sun, X., Ji, Z., & Luan, Z. (2012). Preparation and properties of PVDF composite hollow fiber membranes for desalination through direct contact membrane distillation. Journal of membrane science, 405, 185-200.

[158] Macedonio, Francesca, Aamer Ali, Teresa Poerio, Essam El-Sayed, Enrico Drioli, and Mahmoud Abdel-Jawad. "Direct contact membrane distillation for treatment of oilfield produced water." Separation and Purification Technology 126 (2014): 69-81.

[159] Gryta, M. (2018). Capillary polypropylene membranes for membrane distillation. Fibers, 7(1), 1.

[160] Zuo, J., Bonyadi, S., & Chung, T. S. (2016). Exploring the potential of commercial polyethylene membranes for desalination by membrane distillation. Journal of membrane science, 497, 239-247.

[161] Mulder, M. (2012). Basic principles of membrane technology. Springer science & business media.

[162] Ahmad, N. A., Leo, C. P., Ahmad, A. L., & Ramli, W. K. W. (2015). Membranes with great hydrophobicity: a review on preparation and characterization. Separation & Purification Reviews, 44(2), 109-134.

[163] Das, R., Arunachalam, S., Ahmad, Z., Manalastas, E., Syed, A., Buttner, U., & Mishra, H. (2020). Proof-of-Concept for Gas-Entrapping Membranes Derived from Water-Loving SiO $ _ {2} $/Si/SiO $ _ {2} $ Wafers for Green Desalination.

[164] Shirazi, M. M. A., Kargari, A., & Tabatabaei, M. (2014). Evaluation of commercial PTFE membranes in desalination by direct contact membrane distillation. Chemical engineering and processing: Process intensification, 76, 16-25.

[165] Ahmad, A. L., Otitoju, T. A., & Ooi, B. S. (2019). Hollow fiber (HF) membrane fabrication: A review on the effects of solution spinning conditions on morphology and performance. Journal of industrial and engineering chemistry, 70, 35-50.

[166] Xu, W., Hu, X., Zhuang, S., Wang, Y., Li, X., Zhou, L. ... & Zhu, J. (2018). Flexible and salt resistant Janus absorbers by electrospinning for stable and efficient solar desalination. Advanced Energy Materials, 8(14), 1702884.

[167] Hu, X., Xu, W., Zhou, L., Tan, Y., Wang, Y., Zhu, S., & Zhu, J. (2017). Tailoring graphene oxide-based aerogels for efficient solar steam generation under one sun. Advanced materials, 29(5), 1604031.

[168] Fu, Y., Wang, G., Mei, T., Li, J., Wang, J., & Wang, X. (2017). Accessible graphene aerogel for efficiently harvesting solar energy. ACS Sustainable Chemistry & Engineering, 5(6), 4665-4671.

[169] Ren, H., Tang, M., Guan, B., Wang, K., Yang, J., Wang, F.... & Liu, Z. (2017). Hierarchical graphene foam for efficient omnidirectional solar thermal energy conversion. Advanced Materials, 29(38), 1702590.

[170] Sajadi, S. M., Farokhnia, N., Irajizad, P., Hasnain, M., & Ghasemi, H. (2016). Flexible artificially-networked structure for ambient/high pressure solar steam generation. Journal of materials chemistry A, 4(13), 4700-4705.

[171] Zeng, Y., Wang, K., Yao, J., & Wang, H. (2014). Hollow carbon beads for significant water evaporation enhancement. Chemical Engineering Science, 116, 704-709.

[172] Zhou, J., Sun, Z., Chen, M., Wang, J., Qiao, W., Long, D., & Ling, L. (2016). Macroscopic and mechanically robust hollow carbon spheres with superior oil adsorption and light-to-heat evaporation properties. Advanced Functional Materials, 26(29), 5368-5375.

[173] Mulder, M. R., & Vrij, A. (1996). Explaining conversation rules to children: An intervention study to facilitate children's accurate responses. Child Abuse & Neglect, 20(7), 623-631.

[174] Aroon, M. A., Ismail, A. F., Matsuura, T., & Montazer-Rahmati, M. M. (2010). Performance studies of mixed matrix membranes for gas separation: A review. Separation and purification Technology, 75(3), 229-242.

[175] Abdul Qadir, M., Shahzadi, S. K., Bashir, A., Munir, A., & Shahzad, S. (2017). Evaluation of phenolic compounds and antioxidant and antimicrobial activities of some common herbs. International journal of analytical chemistry, 2017(1), 3475738.

[176] Bellier, M., Ali, M. E., Abo El fadl, M. M., & Perreault, F. (2024). Photothermal Carbon Black Nanoparticle Coating Increases Scaling Resistance in Solar Membrane Distillation. ACS ES&T Water, 4(12), 5925-5932.

[177] Politano, A., Argurio, P., Di Profio, G., Sanna, V., Cupolillo, A., Chakraborty, S., & Curcio, E. (2017). Photothermal membrane distillation for seawater desalination. Advanced materials, 29(2), 1603504.